Polymer 53 (2012) 4–28

Contents lists available at SciVerse ScienceDirect

Polymer

journal homepage: www.elsevier.com/locate/polymer

Feature Article

Establishment, morphology and properties of carbon nanotube networks in polymer melts

Ingo Alig [a,**], Petra Pötschke [b,*], Dirk Lellinger [a], Tetyana Skipa [a], Sven Pegel [b], Gaurav R. Kasaliwal [b], Tobias Villmow [b]

[a] Deutsches Kunststoff-Institut (DKI), Schlossgartenstr. 6, D-64289 Darmstadt, Germany
[b] Leibniz-Institut für Polymerforschung Dresden e.V. (IPF), Department of Polymer Reactions and Blends, Hohe Str. 6, D-01069 Dresden, Germany

ARTICLE INFO

Article history:
Received 15 August 2011
Received in revised form
28 October 2011
Accepted 28 October 2011
Available online 18 November 2011

Keywords:
Carbon nanotube-polymer composites
Filler network
Electrical conductivity

ABSTRACT

As for nanofillers in general, the properties of carbon nanotube (CNT) -polymer composites depend strongly on the filler arrangement and the structure of the filler network. This article reviews our actual understanding of the relation between processing conditions, state of CNT dispersion and structure of the filler network on the one hand, and the resulting electrical, melt rheological and mechanical properties, on the other hand. The as-produced rather compact agglomerates of CNTs (*initial agglomerates*, >1 μm), whose structure can vary for different tube manufacturers, synthesis and/or purification conditions, have first to be well dispersed in the polymer matrix during the mixing step, before they can be arranged to a filler network with defined physical properties by forming *secondary agglomerates*. Influencing factors on the melt dispersion of initial agglomerates of multi-walled CNTs into individualized tubes are discussed in context of dispersion mechanisms, namely the melt infiltration into initial agglomerates, agglomerate rupture and nanotube erosion from agglomerate surfaces. The hierarchical morphology of filler arrangement resulting from secondary agglomeration processes has been found to be due to a competition of build-up and destruction for the actual melt temperature and the given external flow field forces. Related experimental results from in-line and laboratory experiments and a model approach for description of shear-induced properties are presented.

© 2011 Elsevier Ltd. Open access under CC BY-NC-ND license.

1. Introduction

Although the first electron microscopy observation of hollow graphitic carbon nanofibers was reported by Radushkevich and Lukyanovich as early as 1952 [1] it took more than forty years until the 'coaxial tubes of graphitic sheets' [2] attracted a broad scientific community and found practical application. The multi-walled carbon nanotubes (MWCNTs) consisting of graphitic sheets, ranging in number from 2 up to about 50 were first described in detail by Iijima in 1991 [2]. Interestingly, MWCNTs were already used at this time as 'fibrils' in masterbatches produced by Hyperion Catalysis Inc. (Cambridge, OH, USA) starting with a patent in 1987 [3]. However, after Iijima's paper several other companies around the world started commercial scale productions of multi- or single-walled carbon nanotubes (SWCNTs). Based on their high aspect ratio, strength and remarkable physical properties several engineering applications have been developed [4]. Especially due to their unique electrical properties and the potential for mechanical reinforcement [5] carbon nanotubes (CNTs) were considered to be ideal fillers materials in high performance polymer composites. Adding of small amounts of CNTs can turn an electrically insulating polymer into a conductive composite, which is not possible with the same amounts of conventional (lower aspect ratio or spherical) conductive fillers [6] as e.g. carbon black (CB). This is usually explained by a reduction of the so-called percolation threshold due to the very high aspect ratio of CNTs. Fig. 1 shows exemplarily the difference in the concentration dependence of the electrical conductivity for MWCNTs (high aspect ratio) in polycarbonate and for carbon black (aspect ratio close to one) in natural rubber (adapted from [7] and [8]). Although data from different matrices are compared, the reduction of the so-called "percolation threshold" (p_c) due to a higher aspect ratio of the filler is quite general. The percolation threshold values (p_c) are indicated in Fig. 1 by dotted lines. Details on the samples and the fitting equations (solid lines) can be found in [7,8]. As it will be shown later, in most composites the CNTs are not randomly distributed in the matrix and form so-called secondary agglomerates. In reality, between

* Corresponding author. Tel.: +49 351 4658 395; fax: +49 351 4658 565.
** Corresponding author. Tel.: +49 6151 16 2404; fax: +49 6151 292855.
E-mail addresses: ialig@dki.tu-darmstadt.de (I. Alig), poe@ipfdd.de (P. Pötschke).

0032-3861 © 2011 Elsevier Ltd. Open access under CC BY-NC-ND license.
doi:10.1016/j.polymer.2011.10.063

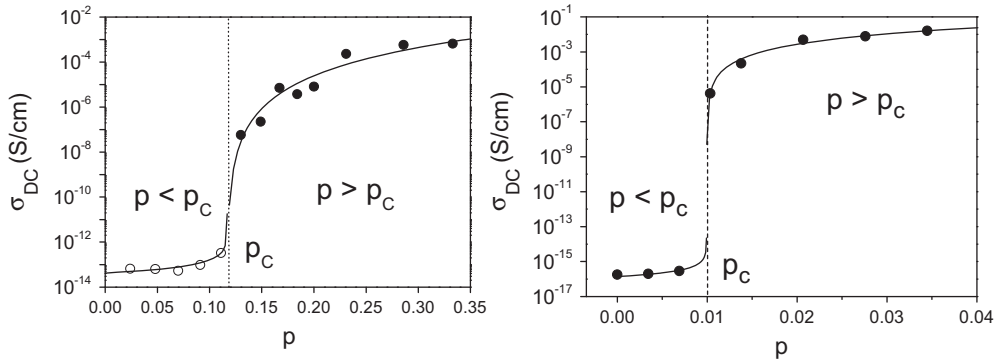

Fig. 1. DC conductivity versus volume content of carbon black in natural rubber (left) and for MWCNTs in polycarbonate (right). The figures are adapted from Refs. [7] and [8].

most nanoobjects weak attractive interactions have to be assumed, which cause agglomeration. Therefore, the basic assumption of percolation theory is not fulfilled and the usual interpretations in terms of classical percolation theory have to be questioned. For that reason, in the following the term 'insulator-conductor transition' is used instead of 'electrical percolation threshold'. To our knowledge the occurrence and importance of agglomeration or clustering of nanoparticles in a polymer matrix was first established by Schulte and co-workers [9,10] for carbon black in epoxy.

By adding only small amounts of CNTs, needed to achieve the insulator-conductor transition, the desired properties of the polymer matrix (e.g. crack resistance, toughness) are usually better preserved than in the case of large amounts needed for conventional fillers like CB. For improvement of mechanical properties and a good balance with other desired composite properties, like processability and surface quality, remaining *initial agglomerates* (normally in the size > 1 μm) have to be avoided, since they act as defects. Therefore, the dispersion of these as-received nanotube agglomerates, sometimes called "primary agglomerates", is an important step toward high quality nanocomposites. Perfectly dispersed CNTs are required for maximum mechanical reinforcement. On the other hand, as will be shown below, the build-up of a conductive network by so-called secondary agglomeration is needed to achieve a high electrical conductivity. However, although remaining initial agglomerates reduce the available amount of CNTs to form conductive pathways, a small amount of those initial agglomerates does not influence the electrical behavior significantly. It is now the aim of this report to discuss the influence of thermo-mechanical history of CNT composites on the electrical, rheological and mechanical properties. In the presented experimental work only industrial available MWCNTs were used. In order to illustrate the interplay between processing condition, structure of the CNT network, and resulting properties, in the first part the focus is on the influence of melt mixing on the disintegration of *initial agglomerates* and the state of CNT dispersion. In the second part the formation of the filler network (*secondary agglomerates)* by thermally-driven or shear-induced agglomeration and its relation to the final properties is discussed. In the last part the knowledge on the competition of destruction and build-up of the filler network is applied for understanding of injection molding as an example for the last step of the processing chain.

2. Background

2.1. Insulator–conductor transition

Since about 1993 several researchers have reported on percolation-dominated conductivity in polymer-carbon nanotube composites in thermosetting and thermoplastic matrices (see e.g. Refs. [8,11–13]). A recent review on the so-called electrical "percolation threshold" in polymer-carbon nanotube composites in different matrix polymers was given by Bauhofer and Kovacs [14]. Apart from the classical application of CNTs for conductive or mechanically reinforced materials, new specific applications of nanotube-filled polymers were proposed during last years, e.g. for gas and liquid sensing [15,16], liquid crystal displays [17], optical transparent films [18], or actuators [19,20].

Electrical, rheological, and mechanical properties in polymer composites are often explained by the formation of a network of interconnected filler particles, which transfer the electrical current and/or the mechanical stress [22,23]. Mechanical stress (in a continuum sense) in the polymer-CNT composites is assumed to be primarily transferred versus the polymer to the filler particle. A direct transfer of stress from one nanotube to another is only expected in the initial (primary) agglomerates (e.g. due to direct CNT entanglements). For the transfer of electrons, interconnected filler particles are also not necessary for tunneling [24].

For understanding the structure and properties of polymer-CNT composites it can be helpful to consider the coexistence of (i) CNT–CNT, (ii) polymer–polymer and (iii) combined CNT-polymer-CNT interactions [21], which is schematically depicted in Fig. 2. Despite the local interactions between nanotubes and the polymer matrix, the polymer mobility is important for the filler arrangement and the effective viscosity of the composite. Hereby the hierarchy of chain mobility is ranging from local motions and Rouse-type modes to the chain reptation [25]. On the other hand,

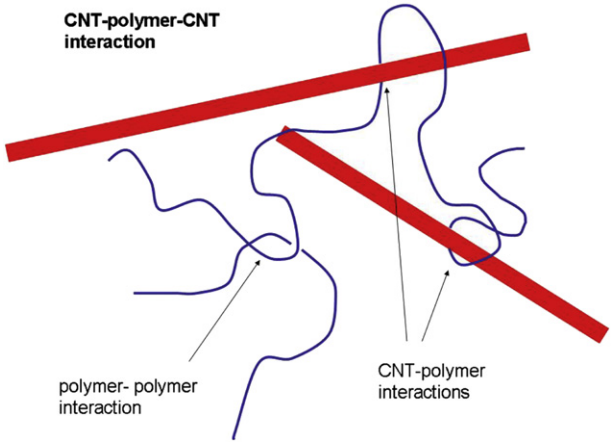

Fig. 2. Illustration of CNT–polymer, polymer–polymer and CNT-polymer-CNT interactions. Figure adapted from Ref. [21].

local CNT-polymer interaction can immobilize the polymer chains in the amorphous regions. Since the CNTs in the polymer matrix usually do not directly touch each other, CNT-polymer-CNT interactions and the "connectedness" [26] play an important role for transfer of the electrical current, the mechanical stress or the phonons (e.g. for "heat conduction"). Therefore, for different properties different types of "connectedness" are of importance. For the case of the "conductive filler network" the tunneling distance of the electrons between neighbored CNTs is assumed to dominate the charge transfer. The mechanical properties are expected to be determined by the combined CNT-polymer network [21]. Assuming at least temporary anchoring of the polymer chains on the nanotubes (e.g. by polymer-nanotube adhesion or wrapping around the CNTs) a chain between two CNTs can act as "entropy spring" in the melt or rubbery state. For heat transport, the CNT-polymer-CNT contacts have to transfer the phonons. The latter may explain the only small increase of the thermal conductivity of composites by adding CNTs which have themselves extremely high intrinsic heat conductivities. However, the detailed nature of CNT-polymer interactions is not clear yet. Despite local molecular interactions also topological interactions (e.g. CNT-polymer entanglements) have to be taken into consideration.

Based on theoretical considerations for statistically distributed filler particles [26–29] the high aspect ratio of CNTs is assumed to enable nanotube percolation at extremely low critical volume fractions p_c. In the limit of large aspect ratios, the relation $p_c \sim 1/(\text{aspect ratio})$ was derived within the excluded volume concept. For a typical CNT aspect ratio of 1000 only about 0.1 vol% are expected to result in percolation. Therefore, as stated above, CNTs were considered to be very attractive filler materials to improve electrical, mechanical and/or thermal properties by adding only small amounts. However, for melt mixed thermoplastics containing CNTs the experimentally determined percolation concentrations (see e.g. Ref. [14]) are often above the theoretical predicted '*statistical percolation*' threshold [26,27,29]. On the other hand, for several other CNT composites – in particularly for such with epoxy matrices [13,30] – percolation thresholds were found which are significantly lower than *statistical percolation* concentrations calculated for the given aspect ratio (see Ref. [14]). The deviation from the predictions of *statistical percolation* threshold is, however, not very surprising, since this concept assumes statistical spatial distribution of the particles, direct contacts between them, and random orientation for non-spherical objects. As stated above, between most nanoobjects – including CNTs – weak attractive interactions have to be assumed, which lead to agglomeration of CNTs in the polymer matrix and formation of a conductive network of interconnected agglomerates/clusters (see e.g. Refs. [31–37]). This was first intensively discussed by Schulte and co-workers [9,10] for CB in epoxy. They attributed the increase of electrical conductivity to the agglomeration of CB induced by external shear forces. Heinrich and co-workers [38] observed agglomeration of layered nanofillers in a thermoplastic matrix and proposed a kinetic equation for the description of the time evolution of the shear modulus.

In addition to nanotube-filled (highly viscous) thermoplastic polymers, there are several works on low viscous colloidal suspensions [39–41] and epoxy resins filled with MWCNTs [42–45]. In those low viscous systems the agglomeration of nanotubes is very pronounced. Agglomeration or cluster formation in general is similar to flow-induced flocculation of particles in colloidal suspensions [46–48]. As stated in [35,36] there is also a remarkable similarity to shear-induced phase separation in polymer blends (see e.g. Refs. [49,50]). The structures of the filler network which appear under shear can lead as well to a notable change in the composite viscosity and conductivity [39,40,42–48]. Furthermore, it was theoretically shown [48] that rigid elongated objects like carbon nanotubes in the presence of shear can agglomerate due to friction forces, even without attraction between them.

Fig. 3 gives an example that the concept of *statistical percolation* does not hold for polymer-CNT composites in general. The left graph in Fig. 3 shows the DC conductivities for a series of injection molded samples before and after annealing for 1 h at 230 °C [32]. The initial samples after injection molding represent a state with almost well-dispersed nanotubes. It is obvious that the shape of the so-called *percolation curve* varies with prehistory. The right graph in Fig. 3 shows the time-dependent increase of the conductivity during annealing, which is ascribed to a time-dependent insulator-conductor transition by formation of conductive agglomerates [32].

In addition to the appearance of agglomerates, CNT are known to be rather worm-like objects with a smaller 'effective aspect ratio' than fully elongated objects, which can also lower the 'percolation thresholds' [51]. Furthermore, CNT can be shortened during polymer melt mixing [8,52] which leads to changes in the length distribution and can also reduce the 'percolation threshold'. An attempt to achieve a more realistic description of the 'percolation' of nanotubes in a polymeric matrix by taking into account the non-ideal characteristics of real CNT (bending flexibility, length polydispersity, attractive interactions) and to overcome at least some of the limitations of the statistical percolation theory [27,29] is made by Kyrylyuk and van der Schoot in [26] who applied the continuum percolation theory of physical clusters to elongated particles in an effective medium.

2.2. Distribution, agglomeration and vitrification

From a technological point of view, two reasons for an inhomogeneous spatial distribution (arrangement) of the fillers in the

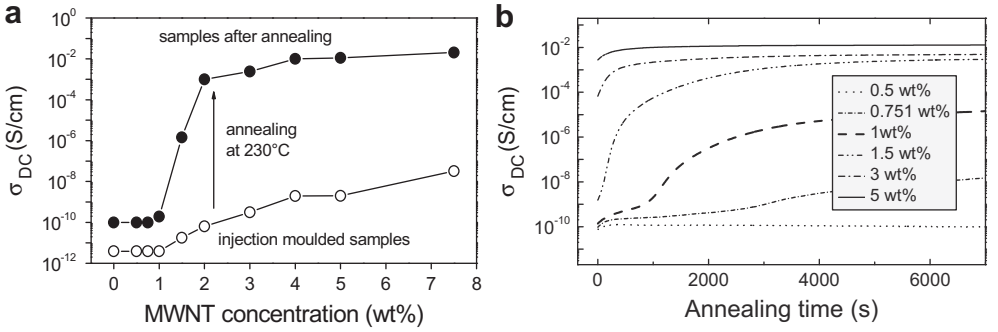

Fig. 3. Insulator–conductor transition for injection molded polycarbonate plates with MWCNTs prior and after annealing: (a) at room temperature (solid state) and (b) time evolution of the conductivity during annealing in the melt at 230 °C. The open circles in (a) represent conductivity after injection molding (well dispersed nanotubes), whereas the filled circles indicate the conductivity after annealing for about 5 h at 230 °C (redrawn from Ref. [32]).

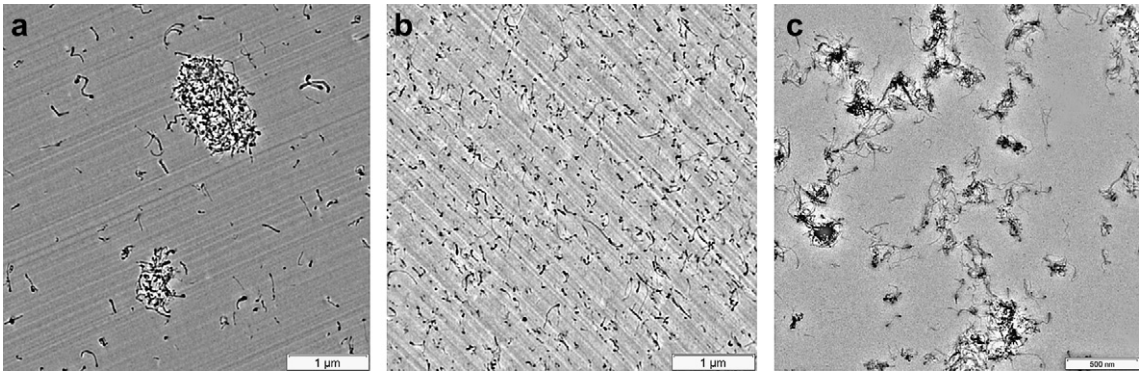

Fig. 4. TEM images of different MWCNT arrangements in a polycarbonate matrix: (a) *Initial agglomerates*, (b) *well dispersed* MWCNTs and (c) *secondary agglomerates*. Replotted from [57], where details of the sample preparation and prehistory are described.

polymer-CNT composites can be considered: (i) insufficient distribution of the filler particles in the mixing process and (ii) secondary agglomeration or cluster formation of initially dispersed filler particles by particle diffusion and external forces (e.g. shear deformation or electrical fields). The latter effect is also described by non-Brownian diffusion of particles with attractive interactions. Both effects, dispersion and secondary agglomeration, are of central importance for understanding the relationship between thermo-mechanical history, the resulting morphology of the filler network (spatial filler distribution in the matrix) and the final properties.

Although several researchers reported on CNT orientation in low viscous polymers (e.g. polysiobutylene, $\eta_0 = 0.5$–10 Pas) or uncured epoxies [53–55], those effects are expected to be dominant only at very high deformation rates (e.g. in melt spinning) and/or if the orientation is frozen very fast (e.g. close to the surface of injection molded parts). Even for polymer melts with higher viscosities (e.g. polycarbonate, $\eta_0 = 10^2$ Pas) the use of shaping techniques with different effective shear rates (10–10^5 s^{-1}) indicated flow induced orientation of MWCNTs to be significant only in the case of micro-injection molding with shear rates above 10^5 s^{-1}, as investigated using TEM from the middle of the samples [56]. Although it cannot be excluded, we consider CNT orientation in the whole composite volume as an effect of second order for polymer melt processing under moderate conditions. A more detailed discussion of the relation between agglomeration/re-agglomeration, on the one hand, and orientation on the other hand will be given in Section 4.7 below.

Considering the production chain starting from melt mixing to the extruded semi-finished goods or injection molded plastic parts, the *initial agglomerates* (Fig. 4a) of the filler have to be first well dispersed in the polymer matrix (Fig. 4b). During the second processing or shaping step (extrusion, injection molding, compression molding, spinning) the final filler network is formed by *secondary agglomerates* or *clusters* (Fig. 4c), which then determines the final properties. It has been experimentally established that the so-called *secondary agglomeration* of CNT can occur in the quiescent melt as well as under shear deformation [31–36]. The *secondary agglomeration* leads to the formation of inhomogeneous conductive filler networks (including '*hierarchical filler structures*') and is considered to be a key process for understanding the dependence of electrical conductivity on thermal and rheological prehistory.

The conductive filler arrangement created in this process is finally 'frozen' by the glass transition, when the melt is cooled down to room temperature, or in the case of thermosetting or other reacting systems, by gelation and/or reaction-induced glass transition. For semi-crystalline polymers, the conductive filler arrangement might be frozen as well, either because the CNTs nucleate crystallinity and are included in the crystals or because of topological restraints in the remaining amorphous phase. Fig. 5a and b show exemplarily the influence of thermal history on the electrical conductivity in an amorphous matrix polymer (polycarbonate (PC) with 1 wt% MWCNT) and a semi-crystalline polymer (polypropylene (PP) with 2 wt% MWCNT). After heating the PC-CNT composite (Fig. 5a) above the glass transition temperature of the matrix polymer, T_g, the secondary agglomeration starts and leads to an increase of conductivity. By cooling below T_g the conductive filler network is frozen in the glassy polymer matrix. Interestingly, the conductivity in the glassy state is slightly increasing during cooling,

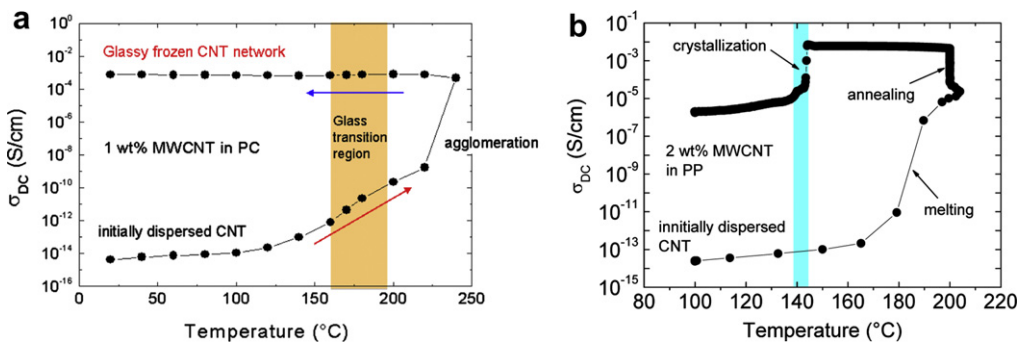

Fig. 5. Electrical conductivity of (a) an amorphous and (b) a semi-crystalline polymer-MWCNT composite during heating-annealing-cooling cycles. The conductivity change in (a) is related to heating above the glass transition temperature (T_g), annealing of the melt and cooling below T_g of a PC-CNT composite (1 wt% MWCNT). In (b) the conductivity changes for PP with 2 wt% MWCNT are shown during melting, isothermal annealing and crystallization (redrawn from Ref. [7]).

which can be explained by thermal shrinkage of the PC matrix which reduces the distance between the CNTs.

An example for the 'fixation' of the conductive network in a semi-crystalline polymer (PP with 2 wt% MWCNT) is shown in Fig. 5b [7]. After very fast heating from 100 °C to 200 °C, which is above the melting temperature of polypropylene ($T_m \approx 145$ °C), the sample was annealed for 5 h. The sample was then cooled below the crystallization temperature with 0.2 K/min. The initial conductivity at 100 °C represents a situation, where the CNT network was (at least partially) destroyed by the squeeze flow during compression molding. During melting and isothermal annealing the sample undergoes an insulator-conductor transition which can be related to *secondary agglomeration*. During cooling the polypropylene crystallizes and the CNT network is 'trapped' in the semi-crystalline structure. The stepwise decrease of the conductivity during crystallization is explained by the reduction of the matrix conductivity due to immobilization of charge carriers.

3. Dispersion of initial nanotube agglomerates

3.1. MWCNT material structure

In order to use the excellent intrinsic properties of carbon nanotubes, in a first step the initial agglomerates have to be disintegrated and the CNTs have to be well dispersed in the matrix. In this context, the dispersion process of MWCNT materials refers to the individualization of the supplied nanotube material into the smallest dispersible unit, namely single carbon nanotubes, within the polymer matrix. However, due to the synthesis process of MWCNT materials, they are usually provided in a strongly agglomerated state, named initial (primary) agglomerates. In these agglomerates the nanotubes are hold together by physical entanglements due to structural defects during their growth and van der Waals interactions between them. Especially in case of fluidized bed methods used in large scale MWCNT production, curved, entangled, and intertwined tubes can be generated strongly deviating from the idealized shape of a cylinder. Such initial agglomerates can possess very high cohesive strength and may be difficult to disperse. Fig. 6 presents exemplarily the structure of two commercially available MWCNT materials, namely Baytubes® C150P from Bayer MaterialScience (Leverkusen, Germany) and Nanocyl™ NC 7000 from Nanocyl S.A. (Sambreville, Belgium) both produced by a CVD method and having similar diameters of about 10 nm of the single nanotubes [58]. The SEM micrographs of as received nanotube powders illustrate more loosely packed but larger agglomerates for Nanocyl™ NC 7000 having a "combed yarn" structure, whereas the Baytubes® C150P material shows much denser but smaller initial agglomerates with a "bird nest" structure. According to the suppliers, the bulk density of Nanocyl ™ NC 7000 is 60 kg/m^3 [59], whereas that of Baytubes® C150P is reported to be 120–170 kg/m^3 [60]. In difference to the producer's information [59,60], length measurements of single nanotubes using TEM [58] revealed significant differences in the x_{50} value between Nanocyl™ NC 7000 and Baytubes® C150P of 1340 nm and 770 nm, respectively.

3.2. Steps involved in dispersion

Whereas dispersion in a polymer matrix can be done using different techniques, like solution mixing, in-situ polymerization, latex approach and melt mixing, the main dispersion mechanisms are the same. They include *wetting of initial agglomerates* by the polymer, *infiltration* of polymer chains into the initial agglomerates to weaken them, the *dispersion of agglomerates* by rupture and erosion, and the *distribution* of individualized nanotubes into the matrix. These mechanisms occur simultaneously during the mixing and are influenced by the characteristics of nanotubes and polymer

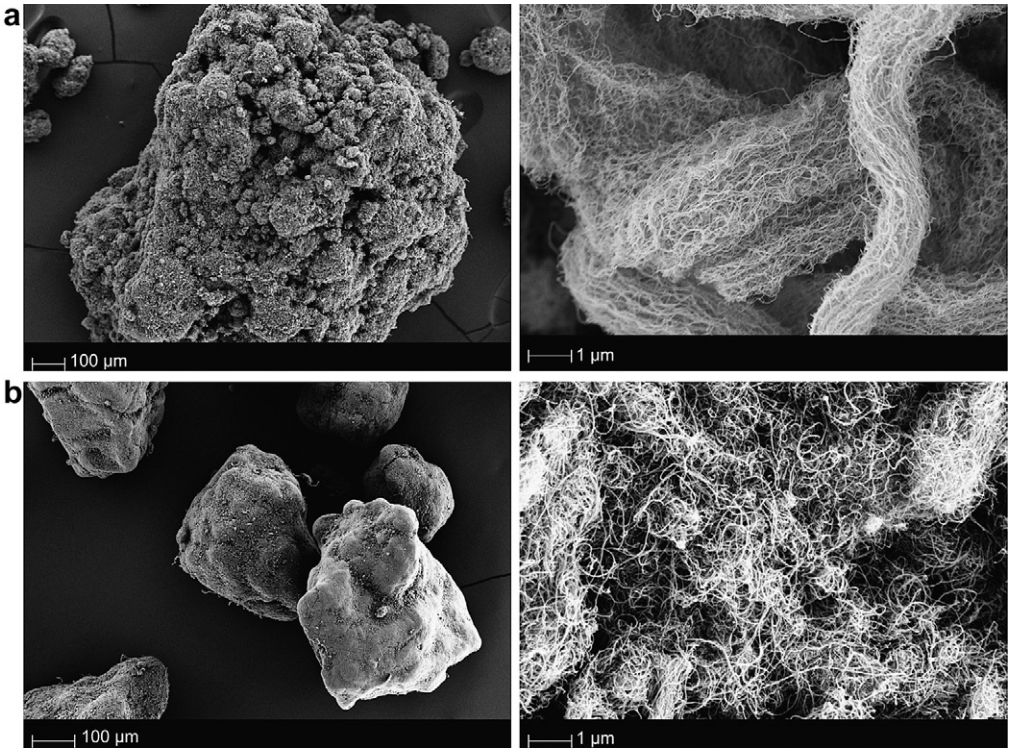

Fig. 6. Scanning electron microscopy images of MWCNT powder at two magnifications: (a) Nanocyl™ NC 7000, (b) Baytubes® C150P. Replotted from [61].

as well as by the choice of mixing procedure and equipment. During these processes, degradation of CNT (mainly by shortening) and of the polymer matrix have to be avoided.

The **wetting of initial agglomerates** in solution or melt depends mainly on the interfacial energy between CNTs and wetting liquids. Especially functional groups on the nanotubes' surface can influence the wetting behavior. In case of nonpolar polyolefin melts already the wetting step can generate problems since MWCNTs are reported to be rather polar [62].

The **polymer infiltration** into the primary agglomerates significantly reduces the agglomerate strength and was found to be important for the following dispersion steps. The infiltration kinetics of a liquid into a porous media can be simplified regarded using the Lucas–Washburn equation. In case of a fully wettable capillary, the time dependent infiltration length $h(t)^2$ is given by (1),

$$h(t)^2 = \frac{r \cdot \gamma \cdot \cos\theta \cdot t}{2\eta_l}, \tag{1}$$

where η_l is the dynamic viscosity, γ is the interfacial tension between capillary and liquid, θ is the contact angle and r is the pore radius. As can be seen from this equation, the infiltration is faster when the pore radius is larger, i.e. for less dense packed agglomerates. It is also faster if the viscosity of the infiltrating liquid is lower, which explains the much faster infiltration of solvents or low viscous thermoset formulations as compared to thermoplastic melts. Since the viscosity of polymer melts depends on shear rate, molecular weight distribution and temperature, the infiltration process can be affected by processing conditions and choice of raw materials. The interfacial tension and the contact angle between the nanotubes and the liquid also influence infiltration, i.e., liquids having surface tensions similar to nanotubes infiltrate better. Finally, the size of the agglomerates determines infiltration time: smaller agglomerates are faster fully infiltrated. Additional effects not considered by the Lucas–Washburn equation are size exclusion (polymer's radius of gyration and pore diameter) and external pressure, which can be present in conventional polymer processing equipments.

The strength of agglomerates σ_M is commonly described using the Rumpf equation (2) [63],

$$\sigma_M = \frac{Z \cdot f \cdot F_H}{O_P}, \tag{2}$$

where Z represents the coordination number of primary particles, f the packing density, F_H the adhesion force and O_P the particle's surface area. However, in case of entangled CNTs the equation of Rumpf cannot be used to estimate the agglomerate strength due to the existence of interlocking. The rupture of agglomerates demands on the breakage or pull out of nanotubes. The number of nanotubes crossing a planar fracture surface can be roughly estimated by means of a stereological approach for isotropic fiber systems [74]. Together with the mean force F_N which is necessary for fiber pull out or breakage the agglomerate strength can be estimated by Eq. (3):

$$\sigma_M = \frac{f \cdot F_N}{2A_0}. \tag{3}$$

Although, real CNT agglomerates exhibit strong deviations from this simple model due to their inhomogeneity and/or anisotropy and the fracture surface is not well defined, some important conclusions can be drawn from Eq. (3). Generally, the tendencies are similar to those according to the Rumpf equation. The agglomerate strength σ_M increases with increasing packing density within the initial agglomerates and with increasing values of F_N (F_H respectively). In the case of failure by CNT pullout, F_N and therefore σ_M increase with increasing number of CNT entanglements and with increasing strength of the attractive forces at the contacts of neighboring CNTs. The number of entanglements itself increases with the length of the CNTs and their packing density within the agglomerates. The attractive interactions between the nanotubes are noticeably reduced if they are infiltrated by a liquid, resulting in a reduced strength of nanotube agglomerates.

Agglomerates are dispersed if the external stress generated by the viscous flow is larger than the agglomerate strength, whereby the latter can be significantly reduced after polymer melt infiltration. The relationship between these two stresses can be characterized by the dimensionless fragmentation number Fa [64]:

$$Fa = \frac{\eta \cdot \dot{\gamma}}{\sigma_M}, \tag{4}$$

with the product of viscosity η and shear rate $\dot{\gamma}$ reflecting the shear stress in case of simple shear and σ_M the maximum strength of the agglomerates. Depending on the value of Fa, different mechanisms for the dispersion of solid agglomerated particles in viscous flow are discussed in the literature. For $Fa >> 1$ rupture or shutter mechanisms are dominant. The rupture mechanism is characterized by breakage of agglomerates into two portions of similar size by separation of the initial particles within a single event. The shutter mechanism results in many nearly equivalently sized smaller agglomerates after reaching a certain stress level, often the level at which smaller agglomerates were compacted before. These dispersion mechanisms are comparatively fast since they progress nearly instantaneously. For $Fa << 1$ erosion of smaller fragments or individual particles from the agglomerate surface can occur. This dispersion mechanism is a comparatively slowly propagating process.

Finally, the smaller agglomerates and eroded individual nanotubes have to be distributed within the matrix melt, whereby the remaining agglomerates continue to undergo rupture and erosion.

3.3. Characterization of dispersion and distribution

To understand or develop processing routes for polymer-CNT composites it is necessary to quantify the nanotube dispersion and distribution within a matrix, which is gained by microscopic techniques. The state of dispersion is commonly understood as the relationship between dispersed (individualized) and non-dispersed CNTs and the degree of dispersion D can be defined as the ratio between the volume fraction of dispersed nanotubes V_{VD} and the total volume fraction V_{VT} of CNTs:

$$D = \frac{V_{VD}}{V_{VT}} \tag{5}$$

Whereas V_{VT} can be assessed from the mass fraction of CNTs and the density ratio of matrix and carbon nanotube material, the estimation of V_{VD} is more difficult. Since in a classical sense only isolated CNTs (not in touch with other CNTs) can be considered as dispersed, the connectivity of every single CNT to its next neighbor has to be investigated. This can be managed practically only by using elaborated techniques such as TEM tomography which offers nanometer resolution. However, in order to gain meaningful information about the composite morphology with more simple and accessible methods, the definition of the term 'dispersion' has to be reduced or differentiated.

Light microscopy (LM) is commonly used to assess the agglomerates in the range of some micrometers and larger but cannot deliver information about agglomeration below this range. Therefore, in LM the fraction of CNTs which cannot be detected is considered as the dispersed fraction. In case of even cuts or thin

sections with thicknesses of a few microns, the area fraction A_A of all remaining initial agglomerates (area ratio) can be used as a relative measure for the non-dispersed fraction. This means only samples with the same total amount of CNTs can be compared. A lower amount of dispersed CNTs is indicated by comparatively higher values of A_A. This quantity has been used as a simple measure for dispersion (the higher A_A the worse the dispersion, [65,66]). Additionally, the agglomerate size distribution, number density [66–68], as well as spatial relationships between the agglomerates [69,70] have been evaluated to gain information about processing-structure-property relationships.

Similar to Eq. (5), the light microscopy based degree of dispersion D_{LM} is described by:

$$D_{LM} = \frac{V_{VD}}{V_{VT}} = \frac{V_{VT} - f \cdot V_{VA}}{V_{VT}}, \quad (6)$$

where $V_{VD} = V_{VT} - f \cdot V_{VA}$ is the volume fraction of dispersed CNTs. V_{VT} represents the total volume fraction of CNTs, V_{VA} the agglomerate volume fraction from LM and f the packing density of CNTs within the agglomerates (space filling factor).

In case of even cuts of the filled composite, V_{VA} is represented by the mean of A_A. In case of thin sections, the mean of A_A increases linearly with the section thickness t. To obtain an unbiased estimate for V_{VA}, the mean of A_A has to be determined for different section thicknesses and extrapolated to zero.

For quantitative evaluation of D_{LM}, the packing density of nanotubes within the agglomerates f is needed, which is difficult to assess. In some investigations a value of 0.25 was assumed (e.g. [67,71,72]). However, it could be shown that this value can vary e.g. for Nanocyl NC 7000 material between 0.07 and 0.25, depending on the compression which may occur during the first steps of melt mixing especially for less compact agglomerates with low bulk densities [73]. The value f may also vary for different nanotubes materials. Thus, the determination of D_{LM} includes a high uncertainty, but it may be used as an approximate value to investigate the effect of different processing conditions for a given nanotube material [72].

The use of transmission electron microscopy (TEM) offers the possibility to directly estimate the volume fraction of dispersed CNTs. Thereby, CNTs which are individualized or part of a loose cluster (packing density significantly lower than in initial agglomerates) are considered as dispersed. CNTs are also allowed to be in touch. For isotropic CNT arrangements the mean of the total length of dispersed CNTs within a unit volume is $J_V = 4 \cdot L_A / \pi \cdot t$, with L_A the mean length of projected CNTs per unit area and t the section thickness [74]. With A_0, the mean cross sectional area of the CNTs, the degree of dispersion is given by:

$$D_{TEM} = \frac{4 L_A \cdot A_0}{\pi \cdot t \cdot V_{VT}} \quad (7)$$

Furthermore, TEM can be used to gain quantitative information about the spatial distribution of CNTs. For this purpose, Pegel et al. introduced the so-called distribution coefficient Q_P which describes the deviation of the filler distribution from a random (Poisson) distribution. It is based on the evaluation of the spherical contact distribution function of the empirical data; details are given in [73]. A value of $Q_P \approx 1$ represents a uniformly distributed coverage probability of CNTs, indicating homogeneously distributed nanotubes. Accordingly, increasing values of Q_P indicate the tendency of CNT clustering resulting in inhomogeneous distribution and can be used to characterize the formation of secondary agglomerates.

3.4. Influences of melt processing conditions on dispersion in small-scale mixing

Beside the nanotubes agglomerate morphology (packing density, nanotube arrangement, see 3.1.), the morphology of single nanotubes (like length, diameter, waviness), the chemical surface structure (like defect quality, functional groups, amorphous carbon layer) and the interactions to the polymer melt, especially the mixing conditions influence the kinetic of the steps involved in the dispersion of initial agglomerates toward individualized nanotubes.

In small-scale batch compounding the influencing factors can be better separated as compared to more complex conditions inside laboratory or industrial scale extruders. Thus, in the following investigations small-scale compounders were used.

The **viscosity of the matrix**, which can be adjusted to a certain extent by the mixing temperature and shear rate, influences the wetting and infiltration behavior as seen on Eq. (1). It can be also assumed that, depending on the agglomerate dimension and the time available for infiltration, the averaged agglomerate strength σ_M in not completely infiltrated agglomerates decreases more when using lower viscous matrices. Due to faster infiltration a higher volume part of the agglomerate is affected. On the other hand, the shear stress applied to the agglomerates is reduced at lower melt viscosities resulting in lower Fa numbers and lower probability of the rupture mechanism. Thus, under constant mixing conditions in most cases more remaining initial agglomerates and worse dispersion are obtained when using lower viscous matrices [68,75]. This is exemplarily shown in Fig. 7 for 1 wt% MWCNT (Baytubes® C150HP) in polycarbonates with different melt viscosities [76]. When plotting the area ratio A_A for different matrix viscosities versus the applied mixing speed (Fig. 8) lower ratios A_A are observed with increasing mixing speed. The similar decrease for different melt viscosities – at least for mixing speeds below 200 rpm – indicate, that the shear stress generated by the mixing speed is of larger influence than the effect of melt infiltration.

As discussed above, for a given polymer grade the **mixing temperature** determines the melt viscosity. An increasing temperature leads therefore to a lower viscosity, a lower shear

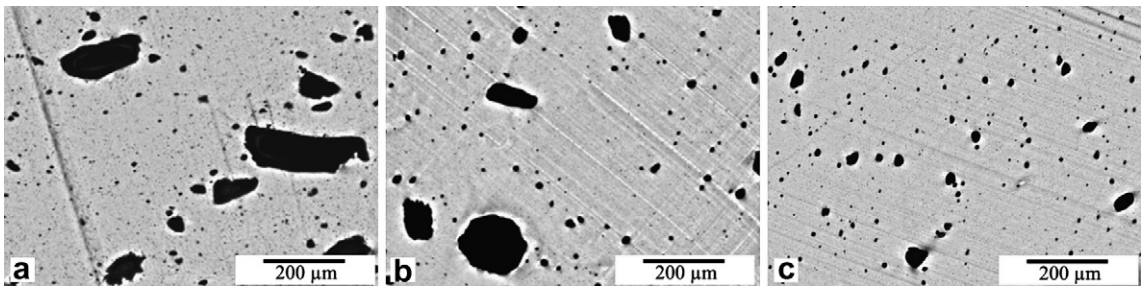

Fig. 7. Optical micrographs of polycarbonate with 1 wt% MWCNT (Baytubes® C150HP) where the polycarbonate differs in melt viscosity: (a) low melt viscosity, (b) medium melt viscosity, (c) high melt viscosity. Composites prepared at 280 °C, 50 rpm, 5 min, section thickness 20 µm (reproduced from Ref. [76]).

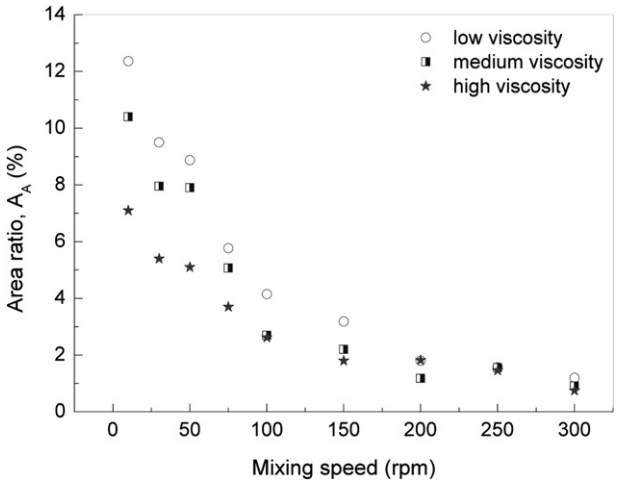

Fig. 8. Area ratio A_A vs. mixing speed for composites of PCs with different viscosity and 1 wt% Baytubes® C150HP (adapted from Ref. [66]).

stress, τ_S, and a worse dispersion [77]. This is illustrated for PC based composites with 1 wt% MWCNT by decreasing values of D_{TEM} in Fig. 9 for mixing temperatures above 240 °C. However, at 220 °C a lower value of D_{TEM} was found, which implies a significant impaired infiltration ability due to the higher viscosity [77]. In general, a competition between the actions of infiltration and shear stress is expected. This can explain the "maximum" in Fig. 9. The distribution coefficient Q_P (Fig. 9b) was found to increase with mixing temperature illustrating increasing agglomeration/clustering tendency on the nanoscale at higher mixing temperatures [77].

When mixing is performed at constant shear stress by adapting the melt temperatures in such a way that constant melt viscosities are given, the importance of the melt infiltration step becomes more obvious. This is illustrated in Fig. 10, where the PC matrix with the lowest molecular weight shows the smallest agglomerates and the lowest agglomerate area ratio as compared to the samples with higher matrix molecular weight.

The **mixing time** influences the completeness of infiltration of initial agglomerates (depending on their structure) and the mixing energy incorporated in the system. In most cases, longer mixing leads to better dispersion. On the other hand, polymer degradation at longer mixing times may induce viscosity reduction or deteriorate the properties of the matrix or the nanotubes. Thus, an optimum between good dispersion and degradation of polymer or nanotube shortening should be found. An example for the influence of mixing time on dispersion is shown in Fig. 11 for 1 wt% MWCNT (Baytubes® C150HP) in PC. At higher mixing speeds lower area ratios A_A are obtained for all mixing times [66]. Interestingly, two time intervals with different slopes are indicated in Fig. 11. Possibly, the steep decrease of A_A in the first 5 min of mixing – indicated for all mixing speeds – is mainly influenced by CNT dispersion dominated by infiltration and rupture, whereas the slower decrease at later times mainly reflects erosion of the remaining smaller agglomerates, even if both occur in parallel. In another study [77], in PC with MWCNTs (Nanocyl N7000) increasing D_{LM} and D_{TEM} values and decreasing Q_P values were approached at longer mixing times. This effect is more pronounced at lower melt temperature and was explained by a better nanotube individualization with increasing mixing time and at lower temperatures (higher shear stresses). For composites of polyamide (PA6) and MWCNTs (Nanocyl NC 7000) at 150 rpm mixing speed increasing D_{LM} values with mixing time (up to 15 min) were reported, however at 50 rpm a maximum was found at 10 min [65]. At both speeds the number of agglomerates decreased with mixing time.

In accordance to Figs. 8 and 11, increasing **screw speed** results in higher shear stress levels and higher fragmentation numbers, so that the fast propagating dispersion mechanisms are promoted. Thus, the dispersion normally increases with the screw speed, illustrated in different systems in smaller and less numerous remaining initial agglomerates (PA12, [75]), lower agglomerate area ratios A_A (PC, [66]), increasing dispersion indices D_{LM} (PC, [72], PA6, [65], PC, [77]) and D_{TEM} (PC, [77]). In addition, with increasing screw speed the distribution coefficient Q_P approaches the value of one indicating increasing homogeneous distribution of the nanotubes (PC, [77]).

The **amount of nanotubes** to be inserted into the polymer matrix also influences the dispersion. On the one hand, at higher loadings the already dispersed nanotubes enhance the matrix viscosity and thus the shear stresses acting on remaining initial agglomerates. On the other hand, a good wetting and infiltration may be restricted if there are too many nanotube agglomerates in the melt. Usually, more and bigger agglomerates are observed when increasing the nanotube amount. However, serious investigations on that topic were not found.

The effect of higher shear forces involved when adding higher amounts of nanotubes is used in the in two-step processing **masterbatch technique**. Here, first a masterbatch with relatively high

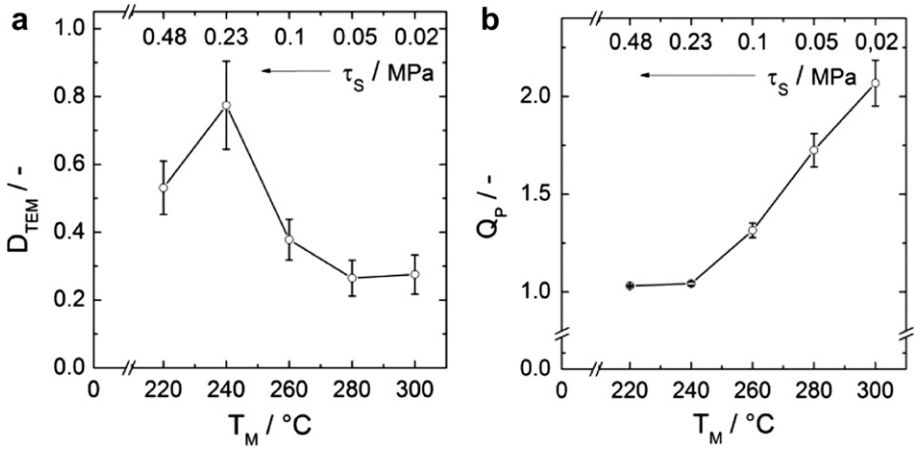

Fig. 9. Influence of mixing temperature T_M on the morphological quantities (a) D_{TEM} and (b) Q_P. The composites of 1 wt% NC 7000 in polycarbonate have been processed by means of a DACA microcompounder with equal screw speed and mixing time (50 rpm and 5 min), the corresponding shear stresses are indicated (reproduced from Ref. [77]).

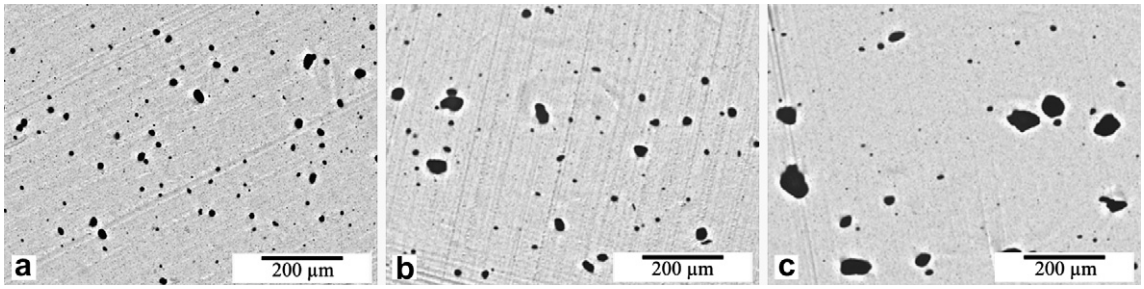

Fig. 10. Optical micrographs of polycarbonate with 1 wt% MWCNT (Baytubes® C150HP) where the polycarbonates differ in molecular weight but show the same melt viscosity: (a) low molecular weight (Makrolon 2205, 240 °C), (b) medium molecular weight (Makrolon 2600, 290 °C), (c) high molecular weight (Makrolon 3108, 310 °C). Composites prepared at 100 rpm, 5 min, temperatures adjusted to obtain a zero shear viscosity of about 500 Pas, section thickness 20 μm, replotted from Ref. [76].

nanotubes loading (typically 10–20 wt%), thus generating high shear forces favorable for dispersion, is prepared. In a second step this masterbatch is molten again to be mixed with pure matrix material for its dilution [78]. For masterbatches in most cases low viscosity matrices are chosen due to the better agglomerate infiltration and the expected high viscosity increase at such high loadings. Miscibility of the matrix and dilution polymer is a requirement for the gradual expansion of the aimed dense network-like nanotube structure in the masterbatch: This was shown clearly in [79] where blend-like structures with nanotubes only in the initial masterbatch phase were found when diluting a PP masterbatch from Hyperion Catalysis International using a maleic anhydride grafted PP. Best dispersion and distribution can be found when using for the dilution the same polymer like in the masterbatch or one with similar rheological properties [79]. In most cases, after a two-step process a better dispersion is found as compared to direct incorporation, which can be assigned to the already described effect of higher shear forces but also to the longer effective mixing time. However, a two-step melt mixing process may cause a more distinctive decrease of the nanotube length, which may negatively influence the electrical percolation and mechanical enhancement.

3.5. Influences of nanotube material and polymer type

As described in 3.1, MWCNT materials from different producers can have different characteristics concerning nanotube and agglomerate morphology and their surface characteristics. As already discussed above, melt infiltration is enhanced if the agglomerate structure is less dense and more open and the wetting with the polymer melt is better. It is also more complete (at given mixing conditions) if the initial agglomerates are smaller. It could be also shown, that agglomerates of nanotubes with shorter length or larger outer diameters can be easier dispersed [76]. This may be explained by higher agglomerate strength of the initial agglomerates in case of thinner and longer nanotubes, since thinner nanotubes have a relatively higher surface area and more interactions between the tubes, whereas longer nanotubes tend to a higher number of contacts and more entanglements between them. In addition, purification of nanotubes may lead to more pronounced CNT–CNT contacts (e.g. to larger van der Waals forces) as compared to nanotubes with amorphous carbon layers on their surface and therefore can show higher agglomerate strength.

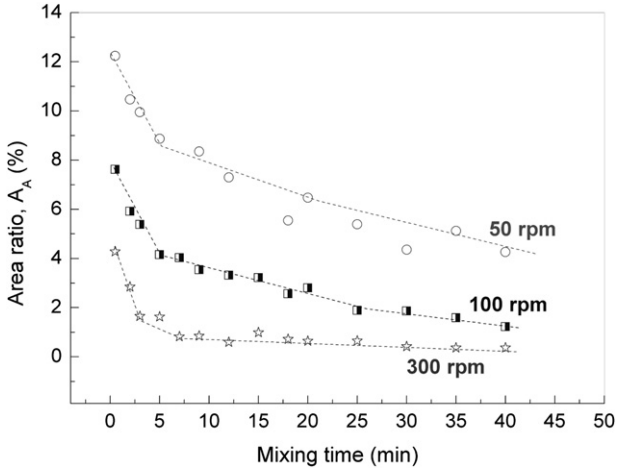

Fig. 11. Area ratio A_A vs. mixing time at different mixing speeds for composites of PC (low viscosity) with 1 wt% Baytubes® C150HP (reproduced from Ref. [66]).

An example of the influence of different nanotube materials in polyamide 12 is shown in Fig. 12, where light microscopy images of composites with 2 wt% MWCNT processed under identical conditions are shown. A simple assignment of the origin of the observed different states of dispersion cannot be done as the quality of the nanotubes differs in more than one parameter.

Another example for the influence of different nanotube materials, related to different structures within the initial agglomerates, is shown for polycarbonate in [57]. The correlation between the dispersability assessed from sedimentation studies of nanotubes in aqueous surfactant dispersions and in polymer matrices was more thoroughly studied in PA6.6 ([80]) and could be confirmed also for other systems (PA12, [75], PC, [52]).

On the other hand, the interactions between CNTs and the polymer matrix play an important role for the dispersion process. Fig. 13 shows an example where 1 vol% MWCNT (Nanocyl NC 7000) were introduced into different thermoplastic matrices using a DACA microcompounder run at 100 rpm for 5 min. The melt temperatures were adapted in such a way that the melt viscosities and thus the shear stresses were constant at 500 Pas (details see Ref. [81]). In Fig. 14 the area ratio A_A obtained from a series of optical micrographs is plotted versus the interfacial energy which was calculated using the harmonic mean equation based on literature values for the polymers and a reference for nanotubes [62].

Even if there is a tendency that the dispersion gets worse with increasing interfacial energy, no general relationship can be found for all polymers, since PS and PMMA deviate from that tendency. This may be addressed to the high chain stiffness of PS and the bulky methyl acrylate side groups in PMMA, which may hinder infiltration and interactions of these polymers with the initial agglomerates. In the ranking of the other polymers, polyolefins having the highest interfacial energy to nanotubes show the worst dispersion. PA6.6 with the lowest interfacial energy shows the best dispersion. The situation is similar when plotting the dispersion index D_{LM} versus the effective Hamaker constant as shown in [81].

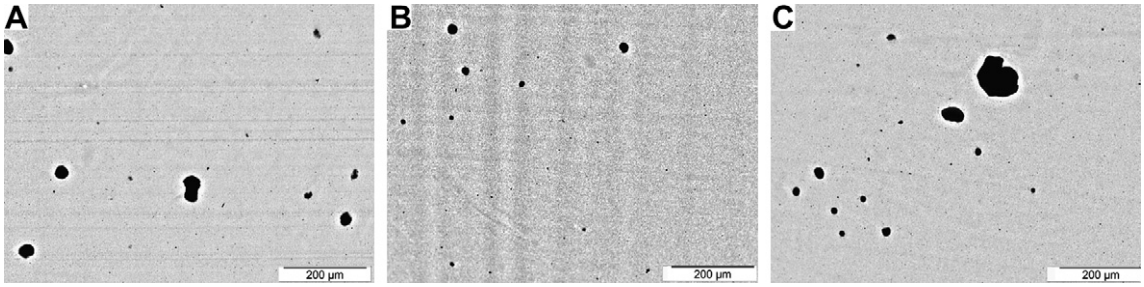

Fig. 12. Effect of different nanotube materials at 2 wt% loading on their dispersion in PA12, light microscopy images (5 µm thin cuts): (A) Nanocyl™ NC 7000, (B) Future Carbon CNT-MW-K, (C) Baytubes® C150P. Replotted from Ref. [75].

3.6. Examples for mixing in continuous extruders

These presented processing-dispersion relationships can be extended to a certain amount also toward melt processing using continuous melt mixing processes like twin-screw extrusion.

Whereas influencing parameters can be separately investigated in batch compounding, they are interrelated in a continuous extrusion process. Thus, increased screw speed or throughput results in shorter residence times, as also different screw designs can do. In order to have measures for the extrusion process, the specific mechanical energy (*SME*) is quite often used, indicating the amount of energy introduced into a unit mass of the material. In case of continuous extrusion processes the *SME* is defined by

$$SME = \frac{2\pi\tau \cdot N}{\dot{m}} \tag{8}$$

where τ denotes the torque necessary for driving the screw, N the screw speed and $\dot{m}$ the throughput. It is generally assumed, that high *SME* increases dispersion as higher shear stresses are generated.

As concluded from small-scale mixing studies, high screw speeds leading to a high shear stress level and long mixing times result in better CNT dispersions. Similar effects were observed recently on twin-screw extruded composites based on poly(lactic acid) (PLA) [67], poly(caprolactone) (PCL) [82], and polycarbonate (PC) [77] with MWCNT (NC 7000) material.

Due to the industrial relevance of the masterbatch dilution technique, detailed investigations were done on the production of high-quality masterbatches with good dispersion. For PLA based composites [67] the processing conditions screw configuration, screw speed, and temperature profile were found to influence CNT dispersion and distribution during the masterbatch production using 15 or 7.5 wt% NC 7000. A rotation speed of 500 min^{-1} that still ensures a certain residence time of the melt combined with a screw profile containing mainly mixing elements were found to be best in dispersing and distributing 7.5 wt% MWCNT in the PLA matrix during both, the masterbatch step as well as the dilution step toward 0.75 wt%.

In a more detailed investigation on the influence of screw configuration, rotation speed, and throughput on the residence time, SME and the resulting macroscopic CNT dispersion performed on PCL based masterbatches with 7.5 wt% NC 7000 [82], the best dispersion was found for an extended screw with $L/D = 48$ (compared to $L/D = 36$), a high rotation speed of 500 min^{-1} and a low throughput of 5 kg/h. The following dilution using the conditions optimized for the masterbatch production step lead to electrical percolated and agglomerate free compression molded samples at 0.5 and 1 wt% loadings.

Whereas in both these studies for the masterbatch step the nanotubes were fed together with the polymer granules into the hopper of a Berstorff ZE 25 extruder, a recent paper [83] indicates, that depending on the nanotube material structure also the feeding

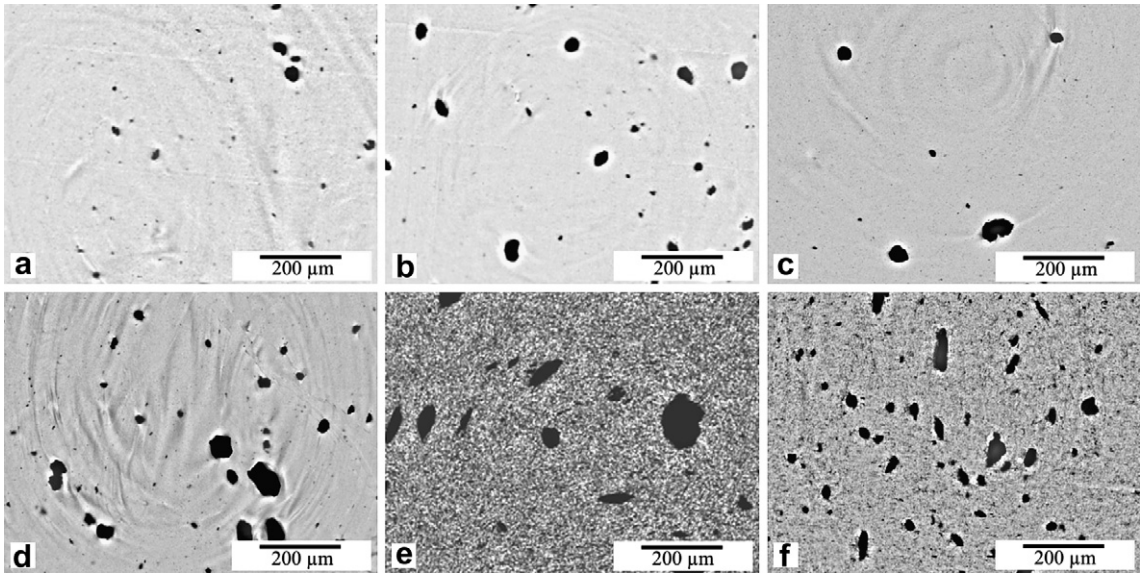

Fig. 13. Effect of polymer matrix material on the dispersion (optical micrographs) of 1 vol% MWCNT NC 7000: (a) PA66 (265 °C), (b) PET (290 °C), (c) PC (300 °C), (d) PA12 (220 °C), (e) PP (200 °C), (f) LDPE (170 °C). Composites produced at 100 rpm, 5 min, processing temperature indicated along with the name of polymer, section thickness 20 µm. Replotted from Ref. [76].

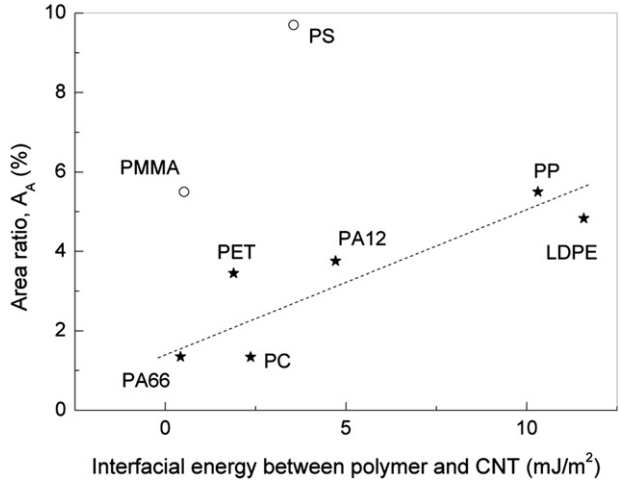

Fig. 14. Effect of polymer matrix type on dispersion, area ratio of remaining initial CNT agglomerates A_A versus interfacial energy between nanotubes and polymer (dashed line is for guiding eyes). Replotted from Ref. [76], details see there.

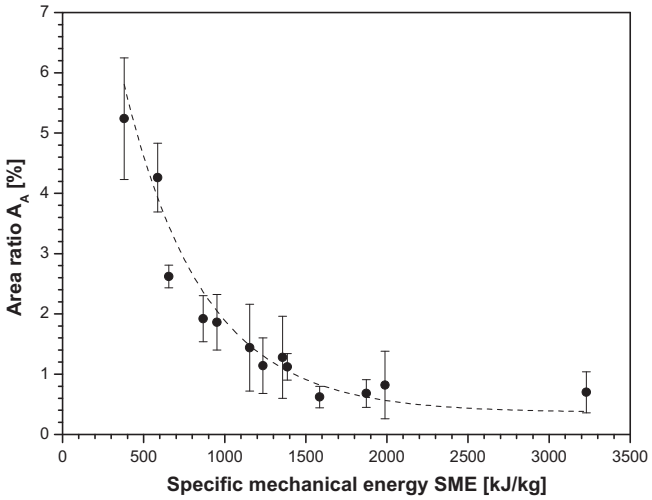

Fig. 15. Relationship between dispersion (remaining initial agglomerate area ratio A_A) and the specific mechanical energy (*SME*) introduced during twin-screw extrusion of polycarbonate based composites with 3 wt% Baytubes® C150P using a Berstorff ZE 25 extruder by varying throughput and rotation speed (A_A from 5 μm thin sections).

conditions have influence on the dispersion. In this study, Baytubes® C150P material with a high bulk density and NC 7000 with much lower bulk density were fed directly either in the hopper or using a side feeder attached at about one third of the length of the extruder into the melt to generate PP based composites. For Baytubes® C150P, feeding together with the solid polymer granules into the hopper resulted in better dispersion, whereas for NC 7000 the use of the side feeder was favorable. This was explained with the finding, that for materials with high bulk density higher shear forces (and longer residence times) are needed for dispersion, whereas the NC 7000 agglomerates with lower bulk density may be compacted when added in the hopper and are more gently dispersed when added in the molten polymer state.

In a recent study by McClory et al. [84] the influence of screw speed during twin-screw extrusion on dispersion and electrical percolation threshold of polystyrene-MWCNT was investigated. The dispersion was best at 100 rpm, whereas also lower dispersion qualities achieved at 20 and 70 rpm lead to comparable electrical percolation thresholds between 1 and 3 wt% addition. The highest mixing speed of 150 rpm led to worse dispersion and a significantly higher percolation threshold.

Detailed investigations concerning the direct MWCNT incorporation were performed using polycarbonate and Baytubes® C150P by varying the throughput and the rotation speed at a given screw (screw 5 in [82]) and temperature profile using a Berstorff ZE 25 extruder. For the composites with 3 wt% C150P, the remaining agglomerate area ratio A_A is plotted in Fig. 15 versus the *SME*, illustrating the strong interrelation between both. Thereby the *SME* increases with rotation speed (varied between 100 and 1000 rpm) but decreases with throughput (varied between 5 and 15 kg/h). On the other hand, the residence times decreased with rotation speed and throughput.

3.7. Nanotube shortening during melt dispersion

It was long time assumed, that carbon nanotubes do not tend to break during melt mixing as due to their hollow structure they show a very high flexibility, unlike carbon nanofibers. However, there were already early indications for a shortening during melt mixing, as decreased conductivity values when prolonging melt mixing time could be explained only by assuming length reduction [8]. Also optical impressions from nanotubes recovered after hydrolysis of the polymer matrix indicated in the case of PA6-MWCNT (NC 7000) nanocomposites shorter tubes after more severe mixing conditions (300 rpm vs. 50 rpm mixing speed at 15 min mixing using a small-scale mixer) [65]. The difficulty to assess the nanotubes length after melt mixing consist in removing the nanotubes without further alteration from the composites in such a way, that length measurements, usually done by TEM, can be performed. As shown earlier, the electrical percolation behavior is discussed in context with the aspect ratio, which reduces with nanotube shortening during processing. Also mechanical reinforcement is connected with the aspect ratio of the reinforcing fibers and was found to be reduced when the aspect ratio of MWCNTs is lower [58]. It may be assumed that the processes of secondary agglomeration are depending on the aspect ratio of the nanotubes as well as the rheological changes with nanotubes addition. In general, it is the aim to retain the high aspect ratio of as-produced nanotubes; even if dispersion is more difficult when having longer nanotubes in the initial agglomerates (see Eq. (3) and its discussion). Shortening is expected to occur mainly on structural defects in the nanotubes walls when the shear forces are exceeding the strength of the nanotubes at such locations. Thus, shortening should be less pronounced in high quality structure nanotubes.

Only recently it got possible to assess nanotubes shortening after melt mixing using the same methodology for investigating as-produced and melt-processed tubes [52]. The industrial grades Baytubes® C150HP and Nanocyl™ NC 7000 were dispersed in chloroform, which was shown to induce a good dispersability as compared to other solvents. Using the same solvent and very mild ultrasonication the polycarbonate matrix of melt processed nanotube composites was dissolved. The nanotube-solvent dispersions were located in a suitable concentration on a TEM grid so that individualized nanotubes could be characterized concerning their length distributions using image analysis. The applicability of this method was shown for two different composites based on different PC and CNT types produced under different conditions. Surprisingly, in both cases a significant shortening to values of 50% (initially shorter Baytubes® C150HP) and 30% (initially longer Nanocyl™ NC 7000) of the initial length was found. An example is shown for Baytubes® C150HP in Fig. 16.

Some more quantitative results were reported for composites with ball milled nanotubes [85]. Whereas the dry grinding of MWCNTs (NC 7000) in a ball mill led to reduction of the length to

54% (after 5 h) and 35% (after 10 h), the melt mixing into polycarbonate using two-step twin-screw extrusion (masterbatch approach) resulted in shortening up to 31%, 50% and 66% of the different initial nanotubes lengths. Thus, in future investigations attention should be paid not only to the state of nanotube dispersion but also to retain the CNT length.

3.8. Concluding remarks how to achieve good dispersion of initial agglomerates

The remaining initial nanotube agglomerates reduce the amount of nanotubes available for electrical percolation and act as imperfections in mechanical tests. Therefore, it is important to obtain individualized nanotubes by melt mixing. The dispersion process is mainly governed by *wetting* and *infiltration* of the melt into initial agglomerates and the dispersion steps *rupture* and *erosion*. Nanotube materials with smaller and more loosely packed structure offer advantages in the infiltration step. Dispersion is assumed to be also more effective, if the interaction between polymer and nanotubes promotes wetting and infiltration. Interactions can be improved by modifying the nanotube's surface (e.g. plasma modification) or the polymer matrix, like adding functional groups, e.g maleic anhydride, or adding compatibilizer/dispersing agents. Shorter and thicker nanotubes are more easily to disperse which is connected with lower agglomerate strength. However, in most cases, length, diameter and packing density are interrelated and cannot be influenced separately.

High mixing energy and long residence time (both are interrelated in extrusion processes) were found to be the most important factors achieving good dispersion. However, high values of both may lead to nanotube shortening, which was not investigated in detail so far.

During the mixing processes it can be assumed that the later described processes of secondary agglomeration already simultaneously occur to a certain extent, especially if low shear stresses are applied in certain zones of the extruder.

4. Thermally-driven and shear-induced agglomeration

4.1. Agglomeration and thermal history

As already discussed in the introduction (see Figs. 3–5), samples with well dispersed nanotubes show usually a lower conductivity as compared to those after *secondary agglomeration* due to thermodynamic driving forces or external forces (here: shear deformation). This can be explained by polymer chains within the contact regions of CNTs which 'insulate' the individual CNTs [21,31,33]. It has been further argued that a *secondary agglomeration* process [31–37] is needed to create a conductive 'superstructure' built by agglomerates or clusters. In these papers it has been assumed that the *secondary agglomeration* leads to an inhomogeneous nanotube distribution with regions having higher CNT concentrations and correspondingly smaller distances between CNTs. Such regions are regarded as *secondary agglomerates*. Alternatively, the picture of a fractal type of structure applies. For very small inter-particle distances (smaller than a few nm) tunneling of electrons between CNTs is expected to reduce the contact resistance [24,86–89]. Although the tunneling is assumed to be the dominant mechanism between the CNTs, the charge transport in the polymer matrix (ion conductivity, electron hopping) has also to be taken into consideration. Even if we show in this section mainly results on MWCNTs in polycarbonate, the following arguments are quite general. The same type of behavior has been found also for other matrices (e.g. PP, PE, PCL and PA) and CNT materials. Differences in the specific interactions can alter kinetic constants of CNT rearrangements and the absolute values of the final properties, but do not change the general character of the underlying mechanisms.

As an example, the dependence of the AC conductivity of compression molded plates (0.6 vol% MWCNT in PC) on the compression molding temperature and the resulting CNT arrangement are illustrated in Fig. 17. Details of the mixing and pressing conditions can be found in [57]. The graphs show the frequency dependent conductivity and corresponding TEM images illustrate the states of CNT distribution. The lower micrograph shows a sample with homogeneously distributed individualized nanotubes, where the '*initial agglomerates*' are destroyed by melt mixing at 250 °C (15 min with 50 rpm, small-scale compounder). This state is well preserved after pressing at 250 °C with a velocity of 6 mm/min. The DC conductivity ($<10^{-16}$ S/cm) of this sample is in the order of magnitude of the neat polymer. The sample prepared from the same composite material but compression molded at 300 °C (6 mm/min) with an electrical conductivity of 5×10^{-4} S/cm represents an inhomogeneous nanotube distribution with secondary agglomerates. The more homogeneous distribution in the lower micrograph is related to the higher viscosity at 250 °C which prevents formation of '*secondary agglomerates*' by higher shear forces. On the other hand, the lower viscosity at 300 °C has

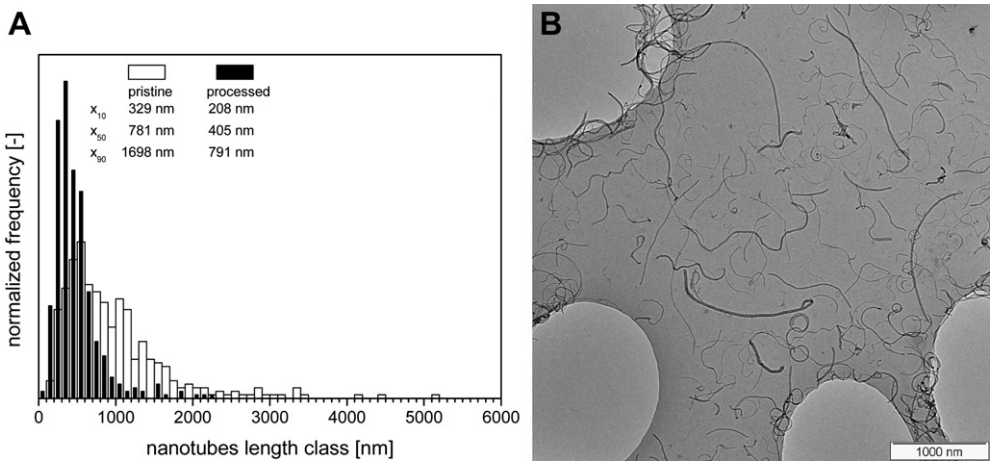

Fig. 16. Comparison of length distribution of Baytubes® C150HP before (pristine MWCNTs) and after processing (as recovered from a melt-processed PC composite with 1 wt% MWCNT) including a TEM image of pristine Baytubes® C150HP. Replotted from Ref. [61], composite preparation: PC, DACA microcompounder, 280 °C, 300 rpm, 5 min (see Ref. [66]).

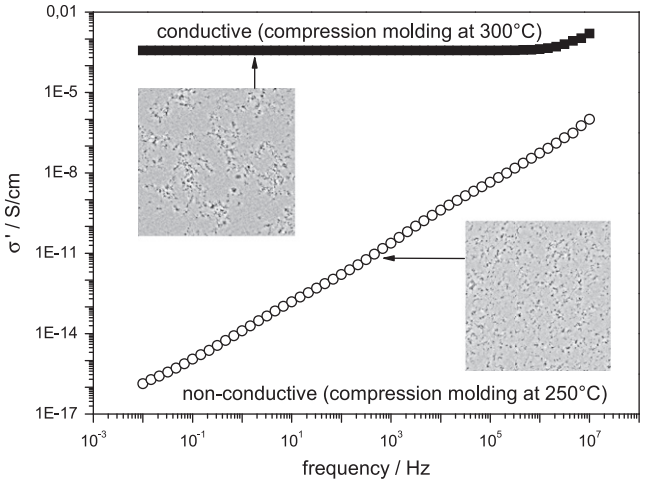

Fig. 17. Frequency dependent conductivity of compression molded polycarbonate/MWCNT plates (0.6 vol% MWCNT, obtained by masterbatch dilution at 250 °C) and the related TEM micrographs (insert): The sample with low conductivity (open circles) represents homogeneously distributed invidualized nanotubes after compression molding at 250 °C. The conductive sample (closed symbols) represents an inhomogeneous nanotube distribution with secondary agglomerates after compression molding at 300 °C. The initial state of dispersion and distribution after melt mixing was similar to that of the low conductivity sample. Adapted from Ref. [57], details see there.

been found to accelerate nanotube agglomeration during compression molding [57].

The acceleration of secondary agglomeration by increasing temperature in the quiescent melt of a PC/MWCNT composite with 0.6 vol% MWCNT is illustrated in Fig. 18. The time-dependent conductivity measurements were performed using a rheo-electrical setup described before [31,33]. In Fig. 18a the experimental procedure is illustrated: By isothermal annealing for 2 h at 230 °C (without shear) of the as-prepared sample an agglomerated initial state has been prepared. This is indicated by a conductivity increase by about three orders of magnitude [31,33]. In the second step the network of agglomerated CNT is destroyed - at least partially - by a well defined short shear pulse (duration: 10 s, shear rate: $\dot{\gamma} = 1\ s^{-1}$). The shear-induced destruction is followed by reformation of the conductive filler network in the quiescent melt ($t > 120$ min). As it has been shown in [36] (see Fig. 6 there) the dynamic shear modulus G' shows also an increase in the same time interval. However, whereas the electrical conductivity increases by about 6 orders of magnitude, the shear modulus increases only from about 60 Pa to about 1000 Pa. This supports our assumption that the mechanisms of stress transfer ("modulus recovery") and charge transport ("conductivity recovery") in the combined polymer-filler network are different. Whereas the electrical properties are rather related to the contact regions between the tubes (length scale of the tunneling distance), the mechanical properties seem to be strongly influenced by the coupling between the fillers via the polymer chains.

In Fig. 18b the conductivity increase in the quiescent melt (second step) is shown for different melt temperatures. The acceleration of the conductivity increase can be explained by a thermal activation of nanotube diffusion which seems to be dominated by the viscosity of the matrix. However, from the available data one cannot identify the diffusion mechanism (transversal, rotational, Fickian, non-Fickian etc.). Similar temperature dependence for the "conductivity recovery" has been found before for MWCNT in different polymer matrices by in-line measurements during extrusion [34]. In these experiments the conductivity was found to increase by several orders of magnitude, after the extruder was stopped.

4.2. Shear-induced agglomeration and de-agglomeration

As shown in Fig. 18, rheo-electrical experiments combining measurements of electrical conductivity and rheological properties under well-defined shear conditions can provide a deeper understanding of the underlying physical mechanisms of the CNT network formation and destruction. To our knowledge those experiment where first time applied to CNT-polymer composites by Migler and co-workers [90,91] who showed a reduction of electrical conductivity and viscosity under steady shear flow. The break-down of the conductivity for a wide variation of shear rates and MWCNT concentrations was somewhat later observed in [91] for PP/MWCNT composites. Somewhat later our group showed time-resolved rheo-electrical experiments during *thermal annealing* (see Section 4.1) and during *transient shear and steady shear deformation* on MWCNTs in PC [31,33,35–37]. The conductivity measurements shown in the following were performed combining an electrometer or an impedance analyzer for measurement of DC and AC conductivity, respectively, with a laboratory rheometer (ARES, Rheometric Scientific). The experimental setup for combined measurements of the dynamic shear modulus and the DC conductivity is schematically represented in Fig. 19. The rheometer tools (plate–plate geometry) act as electrodes [31–33]. In most experiments ring electrodes were used to obtain better defined shear rates in the region of the electrical field.

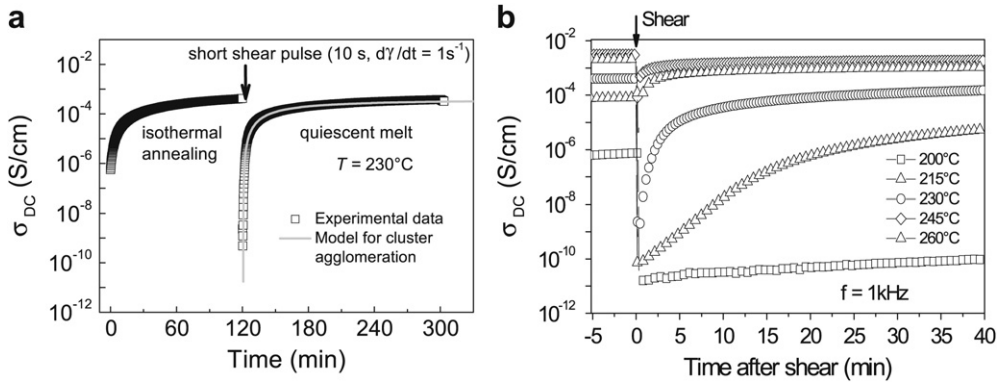

Fig. 18. (a) Conductivity during different stages of the rheo-electrical experiment (isothermal annealing – short transient shear deformation – isothermal annealing) [31,33] and (b) temperature dependence of the conductivity recovery for polycarbonate with 0.6 vol% MWCNT in a rheo-electrical setup with ring electrodes. The model equations for the fit of the "conductivity recovery" (gray line in **a**) are explained in Section 4.3.

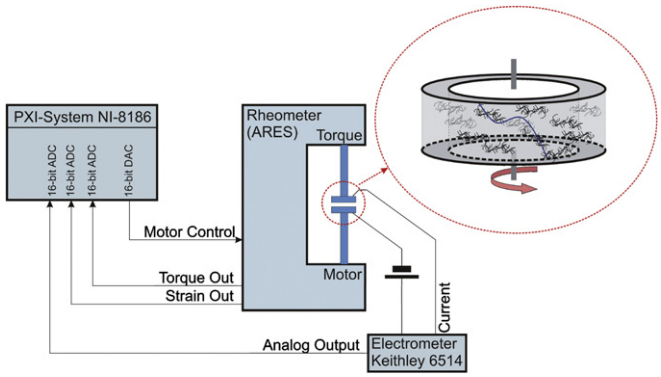

Fig. 19. Schema of the experimental setup for combined measurements of the dynamic shear modulus and DC conductivity.

To study the shear-induced destruction and build-up of the conductive filler network, time-dependent conductivity measurements have been performed for a PC/MWCNT composite with initially agglomerated (Fig. 20a) and dispersed MWCNT (Fig. 20b).

The sample with agglomerated MWCNT (Fig. 20a) was prepared by 1 h of isothermal annealing similar to the first step in Fig. 18a. Then a steady shear deformation with a small shear rate of 0.02 s^{-1} was applied for 1 h; followed by isothermal annealing without shear. During 1 h of steady shear the conductivity approaches a dynamic equilibrium state of the filler network. As expected the conductivity in the quiescent melt increases due to reformation of the CNT network [35,36]. In case of the initially well-dispersed nanotubes (Fig. 20b) an injection molded sample was fast heated to 230 °C in order to keep the CNT almost dispersed and then the shear-stimulated agglomeration of the CNTs was investigated. In comparison to a much slower increase in the quiescent melt (not shown), a small shear deformation (0.02 s^{-1}) can already induce and accelerate an insulator-conductor transition with a conductivity increase by about 6 orders of magnitude. The formation of the network in external shear fields can be explained by a 'picking-up' mechanism under steady shear [35,36]. In the process the nanotubes in a shear gradient are collecting other nanotubes on their way and sticking to each other. This mechanism is different from the nanotube network formation driven by Brownian diffusion of attractively interacting nanofillers. As will be shown in Fig. 30 (below), CNT orientation in the shear flow can be almost neglected for the shear rates used here.

In Fig. 21 the time development of the DC conductivity under steady shear (shear rate: 0.02 s^{-1}) is compared for four samples (same material with 0.6 vol% MWCNT in PC) with different degrees of initial secondary CNT agglomeration. The samples with 'dispersed', 'intermediate' and 'agglomerated' nanotubes were prepared by different durations of agglomeration; for details see Refs. [35,36]. Interestingly, all four samples approach for sufficient duration of steady shear flow the same value of the electrical conductivity. This steady conductivity value is assumed to represent a dynamic equilibrium state of the conductive filler network [35,36].

The same experimental procedure has been applied more recently to MWCNTs in an untreated epoxy matrix (0.1 wt% MWCNT in bisphenol-A-based epoxy resin) as shown in Fig. 22; for experimental details see Ref. [92]. Again, the sample with 'dispersed' and 'agglomerated' CNTs approach the same value of the electrical conductivity after a sufficient time of steady shear deformation with a shear rate of 0.5 s^{-1}. Therefore, we assume that the formation of a dynamic equilibrium state of the (conductive) filler network is quite general for (nano) fillers with attractive interaction and independent of the matrix viscosity. It is remarkable that the agglomeration is much faster for the low viscous epoxy (0.5 Pa s at 70 °C) compared to the polycarbonate melt, with a viscosity of 5–10 kPa s at 230 °C. The low viscosity of the epoxy leads to much larger agglomerates, so that the degree of dispersion can be directly observed in the rheo-microscope. The optical micrographs (inserts of Fig. 22) show that the initially differently agglomerated samples approach comparable final states of dispersion with identical conductivities. The solid lines represent fits using the kinetic equation given on the following paragraph.

4.3. Modeling of build-up and destruction of agglomerates

The growth of the conductive network in a polymer melt can be considered in the simplest case as a clustering process in which attractive particles (here: well dispersed nanotubes) interact and create a conductive agglomerate A (see e.g. Ref. [38]). In the quiescent melt this leads to a time-dependent increase of the volume fraction of agglomerates $p_A(t)$:

$$\frac{dp_A}{dt} = k_0 \cdot (p_{A\infty} - p_A) \tag{9}$$

where p_A is the volume fraction of conductive agglomerates, $p_{A\infty}$ is the value for $t \to \infty$ and k_0 is the kinetic coefficient for quiescent agglomeration. For the case of conductive filler particles, these agglomerates are assumed to form a conductive filler network of 'percolated' clusters or agglomerates [31,33,35–37]. For the description of the agglomeration of nanotubes, kinetic equations of *first or second* order kinetics have been tested. However, within the experimental error is not possible to distinguish between both. In

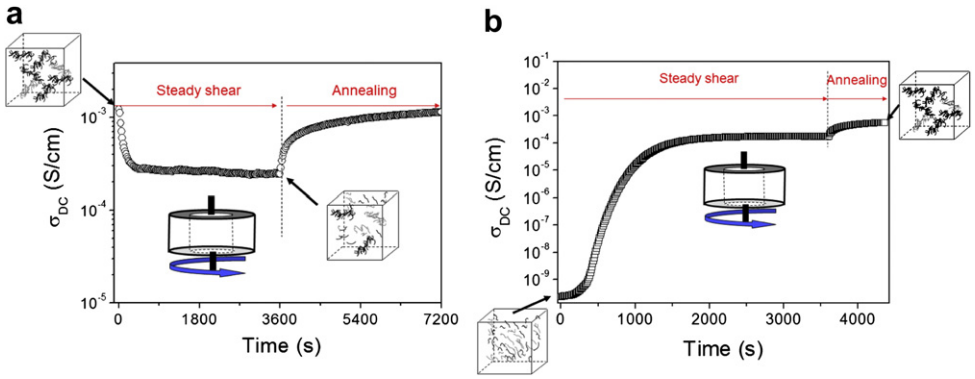

Fig. 20. Time-dependent conductivity for initially agglomerated (a) and well dispersed (b) composites of MWCNT (0.6 vol%) in PC under steady shear deformation ($d\gamma/dt = 0.02\ s^{-1}$ for 1 h) and during quiescent annealing after shear at 230 °C. The inserts schematically show the state of nanotube dispersion and the measuring cell with the sample.

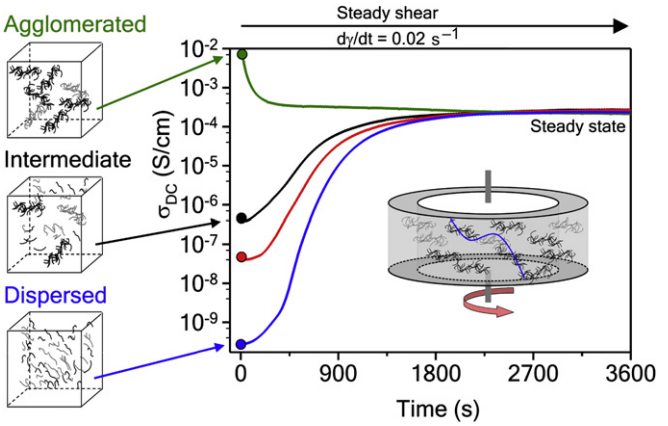

Fig. 21. Time dependence of the DC conductivity under steady shear (shear rate of 0.02 s^{-1} at 230 °C) for four samples (0.6 vol% MWCNTs in PC) with different initially degrees of CNT dispersion.

Fig. 18(a) an example of such a fit (gray line) to the "conductivity recovery" data by combining Eq. (9) with an equation for agglomerate percolation (see Eq. (12) below) is shown. For further details and fit parameters see Ref. [31].

In the case of steady shear a kinetic equation with two shear-dependent terms for shear-induced destruction and agglomeration [31–34] is needed. For the assumption of additivity and first order kinetics one can write:

$$\frac{dp_A}{dt} = k_1(\dot{\gamma})(p_{A\infty} - p_A) - k_2(\dot{\gamma})p_A, \tag{10}$$

where $k_1(\dot{\gamma})$ and $k_2(\dot{\gamma})$ are the kinetic constants for shear-stimulated agglomeration and shear-stimulated destruction process, respectively. The coefficients k_1 and k_2 are assumed to depend on shear rate. Based on Eq. (10) the concentration of agglomerates approaches for steady shear a steady state value

$$p_{A,\text{steady}} = p_{A\infty}\frac{k_1}{k_1 + k_2}, \tag{11}$$

which is determined by the interplay of destruction and build-up effects of the agglomerates [35,36].

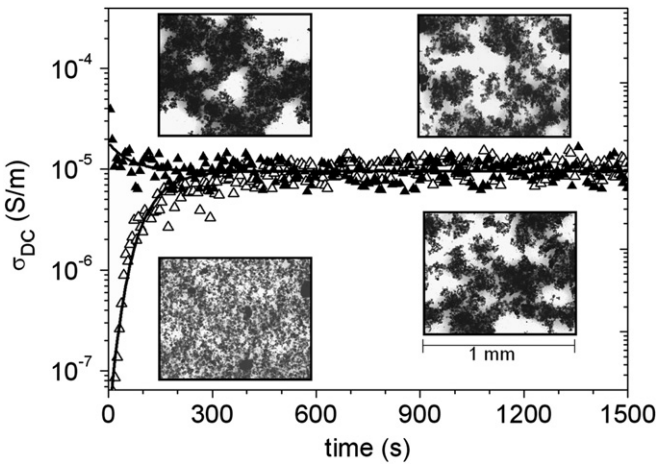

Fig. 22. Time dependent DC conductivity of CNT/epoxy suspensions containing 0.1 wt % MWCNTs at 70 °C at a steady shear rate of 0.5 s^{-1} for two samples with initially dispersed (△) and agglomerated (▲) nanotubes. The inserts show optical micrographs (1 mm width) of the initially and final states for both samples. The solid lines represent fits using the kinetic equation developed in paragraph 4.3, taken from Ref. [92].

For the calculation of the electrical conductivity the solution of Eq. (9) or (10) for $p_A(t)$ can be set alternatively into a 'percolation' equation (e.g. Eqs. (12) and (13)), an expression based on effective medium approach (Eq. (14)) or the modified Fournier equation [31–34]. The filler content $p = p_{\text{filler}}$ in these equations has to be replaced by the time-dependent content of conductive agglomerates $p_A(t)$. For the conductivity values of the filler σ_{filler} and the matrix σ_{matrix} the conductivity values of the nanotube agglomerates σ_A and polymer have to be taken. The value p_c is now the percolation threshold of the 'percolating' conductive agglomerates. It has been established for statistical percolation [93–98], that near the critical concentration p_c the DC conductivity σ_{DC} of the composite follows power laws above and below the percolation threshold p_c:

$$\sigma_{DC} \equiv \sigma'(p, \omega = 0) = \sigma_{\text{matrix}}\left(\frac{p_c - p}{p_c}\right)^{-s}, \quad p < p_c \tag{12}$$

$$\sigma_{DC} \equiv \sigma'(p, \omega = 0) = \sigma_{\text{filler}}\left(\frac{p - p_c}{1 - p_c}\right)^{t}, \quad p > p_c \tag{13}$$

where σ_{matrix} and σ_{filler} are the electrical conductivities of the polymer matrix and the filler. The currently accepted values of the critical exponents s and t [99–102] are $s = t \approx 1.3$ for 2 dimensions and $s \approx 0.73$, $t \approx 2.0$ for three dimensions.

An alternative description of the insulator-conductor transition is the generalized effective medium (GEM) theory (see Refs. [103–105]):

$$(1-p)\frac{\sigma_{\text{matrix}}^{1/s} - \sigma_{DC}^{1/s}}{\sigma_{\text{matrix}}^{1/s} + A\sigma_{DC}^{1/s}} + p_A\frac{\sigma_{\text{filler}}^{1/t} - \sigma_{DC}^{1/t}}{\sigma_{\text{filler}}^{1/t} + A\sigma_{DC}^{1/t}} = 0, \tag{14}$$

where $A = (1 - p_c)/p_c$. σ_{DC}. The simple assumption, that conductive agglomerates form the conductive filler network, has been found to be rather successful to describe the time evolution of the electrical conductivity under shear and in the quiescent melt [31,32,34–37]. As stated above, the filler content p has to be replaced by a time-dependent agglomerate concentration $p_A(t)$ and for σ_{filler} the conductivity of agglomerates$\sigma_{0,A}$ has to be taken. An alternative empirical equation to describe the insulator-conductor transition has been proposed by Fournier et al. [106] and was successfully applied to polymers containing CNT by Coleman et al. [11], Curran et al. [107] and McCullen et al. [108]. This equation was also extended to the assumption of time-dependent agglomerate concentration $p_A(t)$ [32,35,109].

All three approaches (percolation, GEM theory and empirical Fournier equation) were compared for the same set of MWCNT concentrations in PC [32] and in PP [109]. It turns out that all three equations can fit the conductivity data with similar accuracy. In order to keep the advantages of the percolation approach, we made the assumption that the conductive agglomerates, which form the percolation network, are randomly distributed [31]. Since the conductive agglomerate network ('superstructure') is not necessarily built by randomly distributed agglomerates without size distribution, it is obvious that our model is somehow limited.

As shown by Skipa et al. [35] a differential equation with only one variable (as in Eq. (10)) is not sufficient to describe the experimental data. Formally, different sizes of agglomerates (in the simplest case large and small agglomerates and, additionally, separated nanotubes) can be introduced, each with a separate variable for its fraction. Based on Eq. (10) the following system of differential equation for N different types of

agglomerates (e.g. different size or shape, including separated CNTs) can be written:

$$\frac{d\xi_1}{dt} = -k_{1,1}\xi_1 + k_{1,2}\xi_2 + k_{1,3}\xi_3 + \ldots + k_{1,N}\xi_N \quad (15.1)$$

$$\frac{d\xi_2}{dt} = k_{2,1}\xi_1 - k_{2,2}\xi_2 + k_{2,3}\xi_3 + \ldots + k_{2,N}\xi_N \quad (15.2)$$

…..

$$\frac{d\xi_N}{dt} = k_{N,1}\xi_1 + k_{N,2}\xi_2 + \ldots + k_{N,N-1}\xi_{N-1} - k_{N,N}\xi_N \quad (15.N)$$

The boundary conditions are:

$$\sum_{i=1}^{N} \xi_i = 1 \quad (16)$$

$k_{i,j}(\dot\gamma)$ (with $i \neq j$) and $k_{i,i}(\dot\gamma)$ (with $i = j$) are the kinetic constants for build-up and destruction of the agglomerates defined by the indices (i and j). In this model also separated nanotubes are included as one of the fractions. As discussed above in the general case the kinetic constants are dependent on the shear rate and the temperature. The fraction of nanotubes in the i-th agglomerate fraction (ξ_i) is related to the volume fraction of CNT belonging to agglomerates of type i by $p_{A,i}(t) = \xi_i(t)p_{CNT}$, where p_{CNT} is the total volume fraction of CNT in the sample. In this consideration, the large agglomerates disappear due to shear-induced destruction (term: $-k_{i,i}\xi_i$), and appear due to the shear-induced agglomeration of the small agglomerates (term: $k_{i,j}\xi_j$ with $i \neq j$). The agglomeration of separated individual nanotubes (T) can be included by the assumption: $\xi_1 = \xi_T$, $k_{1,1} = k_{T,T} = 0$ and $k_{1,j} = k_{T,j}$. In [35] it has been shown that a simple three-component agglomeration model can already describe a local minimum of the conductivity under shear. An application of Eqs. (15.1)–(15.N) and Eq. (16) to quiescent shear can be done by including terms of the type $k_i\xi_i$. An extension to other types of external deformations (e.g. oscillatory shear) by different initial conditions is also possible. However, real network formation is a much more complicated process and in general all coefficients (k_i, $k_{i,j}$) depend on the shear rate, composite history, temperature, polymer viscosity, etc. Therefore, experimental estimation of those values can be difficult or even impossible. However, the hierarchical set of equations illustrate the network morphology to be a 'hidden parameter'. Therefore, this 'superstructure' (e.g. of fractal-type) should be included in theoretical considerations e.g. by a structure factor of the filler network which depend on the thermo-rheological history.

4.4. Relation between electrical and rheological properties

In the literature different results for the relationship between "electrical" and "mechanical percolation" have been reported [21,23,110–112]. Since the basic assumptions behind the concept of a "percolation threshold" as a function of filler concentration do not apply for *not* randomly distributed particles, it seems to be necessary to consider the relationship between the resulting electrical and rheological properties in more detail. For this reason we combined measurements of electrical and rheological properties. The rheometer was connected to a data acquisition system with an analog output for the motor control [35–37], which allowed overlaying steady rotation (shear rate:$\dot\gamma_{steady}$) and small oscillations ($\dot\gamma(t) = \dot\gamma_0 \sin 2\pi f t$) with frequency f (see Fig. 23, upper graph). From the amplitude and phase of the torque oscillations and amplitude and phase of the strain oscillations the complex shear modulus ($G^* = G' + i\,G''$) was calculated. A strain amplitude of 1% was

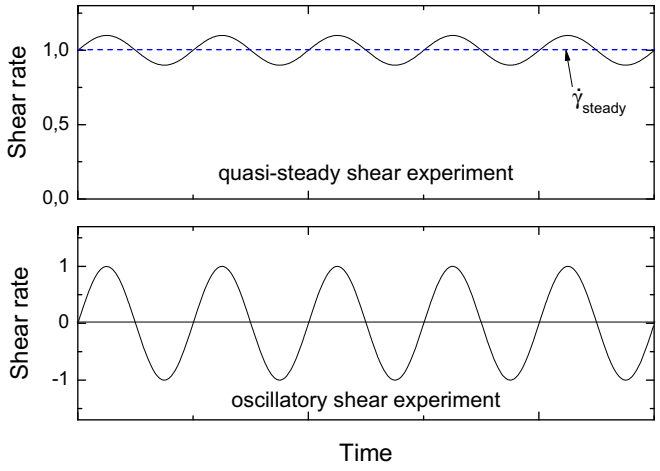

Fig. 23. Schematic representation of the shear rates for a quasi-steady shear experiment (upper graph) and an oscillatory shear experiment (lower graph).

applied. The influence of such small oscillations on the electrical conductivity can almost be neglected [36]. Therefore, although we overlay a small oscillation on top of a constant shear rate, we call this experiment "steady shear" or "quasi-steady shear" experiment with a shear rate $\dot\gamma_{steady}$. The classical oscillatory shear experiment (Fig. 23, lower graph) will be discussed in Section 4.6.

In Fig. 24 the time dependence of the conductivity, as well as G' and G'' are plotted for a PC/MWCNT melt (0.6 vol% MWCNT) during quasi-steady shear ($\dot\gamma_{steady} = 0.02\ s^{-1}$, 230 °C). The initial sample ($t = 0$), prepared by injection molding [35,36], represents a material with almost well-dispersed nanotubes, with an initial low melt conductivity similar to that of PC. When steady shear is applied a tremendous increase of the DC conductivity (as shown before in Figs. 20b and 21) and a simultaneous decrease of G' and G'' is observed. Both processes are related to the formation of a filler network by agglomeration [35,36], which is schematically depicted as inserts. As already discussed above, the formation of a network of agglomerated CNTs is preferential for the electrical conductivity, whereas it is not optimal for the mechanical reinforcement. In order to obtain a conductive pathway in the matrix, an electrical percolation network of *interconnected* conductive particles with very small inter-particle distances, resulting in low contact

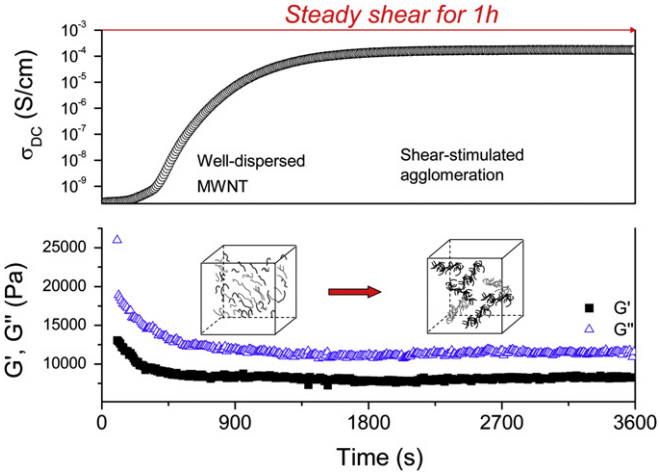

Fig. 24. Shear-induced insulator–conductor (upper graph) transition in a PC/MWCNT melt (230 °C, 0.6 vol% MWCNT) during quasi-steady shear (shear rate: 0.02 s^{-1}) and simultaneously measured storage (G') and loss modulus (G'') (lower graph) [36].

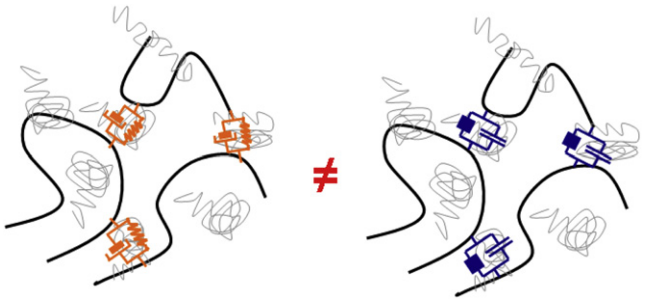

Fig. 25. Schematic representation of the differences between the conductivity ('electrical network') and rheological properties (mechanical active filler network): The shaped nanotubes are represented by black lines and the polymer chains by gray lines. To symbolize the contact resistance an 'electrical equivalent circuit' was taken, whereas the viscoelastic coupling between CNTs via polymer chains is represented by a 'dash pot' for local friction and an 'entropic spring'.

resistances, is needed for an efficient electron transport through the network. On the other hand, for the efficient reinforcement a strong interaction between CNTs and the polymer chains together with a homogeneous space distribution is necessary. The optimal mechanical reinforcement is thus expected for well-dispersed MWCNTs where the available CNT surface and the interfacial region are large. Shear induced agglomeration of nanotubes (see Fig. 24) creates *secondary agglomerates,* which results in a less efficient reinforcement. In other words, 'microfillers' (spherical-like agglomerates) replace well-dispersed 'nanofillers' (individual MWCNTs or small agglomerates). Similar to the conductivity in Fig. 21 the G' and G'' values approach a steady state value for different initial states of dispersion at sufficient duration of shear [35,36]. However, there is another important difference between the behavior of the electrical conductivity and the rheological (G' and G'') properties under shear: the first quantity changes by several orders of magnitude (logarithmic scale), whereas the mechanical properties change only in a linear scale.

The different behavior of electrical and mechanical properties gives a clear indication for the differences in charge transport and transfer of mechanical momentums within the (same) filler network. This difference is not surprising. On the one hand, the electrical current is predominantly carried by the CNT network and the connecting contacts, whereas the conductivity of the matrix is almost negligible. On the other hand, the mechanical forces are transferred in parallel by the CNT network, the polymer matrix, and the CNT-polymer network. For the electrical properties the complex contact resistance (symbolized by an 'electrical equivalent circuit' in the scheme in Fig. 25) seems to be important, whereas the viscoelastic coupling between CNTs and the entangled polymer chains (symbolized by a 'dash pot' for local friction and an 'entropic spring') seems to determine the rheological properties.

4.5. Shear rate dependence and dynamic filler network

In order to investigate the shear-rate dependence of the electrical and mechanical properties a set of PC/MWCNT samples (0.6 vol% MWCNT) with 'agglomerated' MWCNTs and high electrical conductivity were prepared by thermo-rheological pretreatment [36]. Then a constant shear rate $\dot{\gamma}_{steady}$ (in the range from 0.02 to 0.5 s^{-1}), overlaid with a small sinusoidal shear oscillation (as described as a quasi-steady shear experiment in Section 4.4), was applied to each of the samples for a sufficient time to reach constant values for G', G'' and the transient shear viscosity η^+. For calculation of the transient shear viscosity $\eta^+ = \langle\tau(t)\rangle/\dot{\gamma}_{steady}$ the moving average of the torque $\langle\tau(t)\rangle$ (averaged over one period of the overlaid oscillation) was divided by the shear rate $\dot{\gamma}_{steady}$ [36]. After 1 h of shear all quantities reach for each of the shear rates almost constant values, which represent a steady state of the dynamic filler network. The corresponding values of σ_{DC}, G', G'' and η^+ were taken for the steady-state values for $t \to \infty$. In Fig. 26 $\sigma_{steady} = \sigma_{DC}(t \to \infty)$ and $\eta_{steady} = \eta^+(t \to \infty)$ are plotted versus shear rate. The steady state values of σ, G' and G'' (not shown) and η^+ represent a 'dynamic equilibrium' between destruction and build-up of the filler network for the given shear rate. The formation of a 'dynamic filler network' seems to be a general feature for attractive interacting fillers in a liquid matrix (including solid suspensions). The decrease of σ_{steady} and η_{steady} with shear rate in Fig. 26 can be explained by dominance of destruction of the 'conducting' and 'viscoelastic' networks, respectively. A similar shear rate dependence of electrical conductivity and viscosity was reported by Kharchenko et al. [90] and Obrzut et al. [91]. Kharchenko et al. [90] used for description of shear thinning of a PP/MWCNT composite the empirical Carreau equation [113], $\eta(\dot{\gamma}) = \eta_0[1 + (\dot{\gamma}\tau_\eta)^2]^{-n} \propto \dot{\gamma}^{-m_\eta}$, where τ_η and $\dot{\gamma}\tau_\eta$ are the characteristic time and the reduced shear rate, respectively. The decrease of the electrical conductivity was described by an analogous empirical function $\sigma(\dot{\gamma}) = \sigma_0[1 + (\dot{\gamma}\tau_\sigma)^2]^{-n} \propto \dot{\gamma}^{-m_\sigma}$. In these papers the decrease of both transport quantities with $\dot{\gamma}$ was explained by reduction of the number of nanotube contacts by orientation or by disruption in the flow.

The steady state conductivity data were extracted from the data in [36]. For fitting of σ_{steady}, we used a simple semi-empirical equation [36]:

$$\sigma_{stat} = \frac{\sigma_0}{(1 + t_1\dot{\gamma})^t}. \tag{17}$$

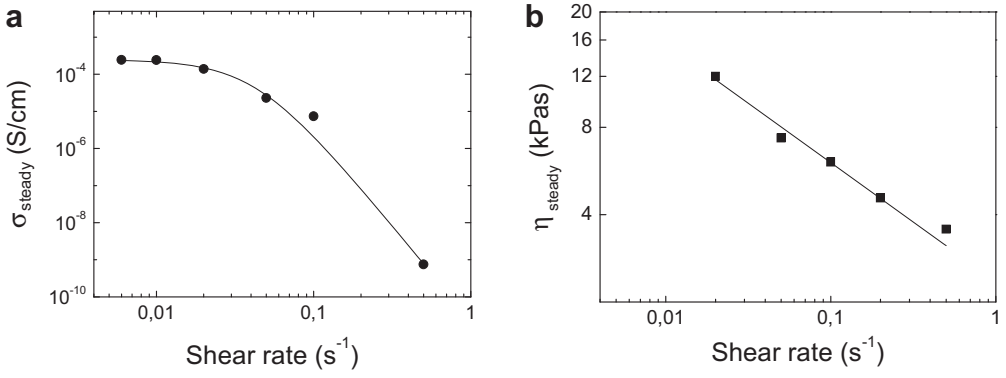

Fig. 26. Steady-state values of the DC conductivity (a) and viscosity (b) vs. shear rate. The lines indicate fits as discussed in the text. For further details see Ref. [36].

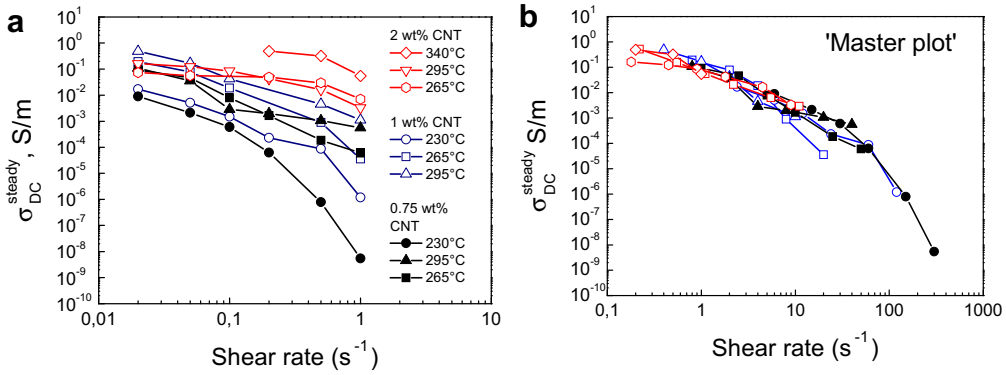

Fig. 27. (a) Steady state conductivity as a function of shear rate at different temperatures and for different MWCNT contents (0.75, 1 and 2 wt%). (b) 'Master plot' construction from the data in the left graph (Reference curve: 340 °C, 2 wt%).

The solid lines in Fig. 26a and b represent the fit with Eq. (17) and the empirical Carreau equation, respectively, as used by Kharchenko et al. [90]. The fit parameters and further details are given in [36].

In Fig. 27a the steady state conductivities for PC/MWNCT compounds of different MWCNT contents (0.75, 1 und 2 wt%), different shear rates (between 0.02 and 1 s^{-1}) and different melt temperatures (230, 265, 295 and 340 °C) are summarized. The data were measured as input parameters for a Finite Element model for calculation of shear-induced conductivity during injection molding [114]. Interestingly, the individual conductivity vs. shear rate curves could be superposed by shifting along the shear rate axis. In Fig. 27b the resulting 'master plot' construction from the data in Fig. 27a is shown. The reference curve (not shifted) is the curve for 2 wt% MWNCT and 340 °C. All other curves are multiplied by a so-called shift factor $a_{T,\Phi}(T,\phi_{CNT})$. Such a 'master plot construction' has been established for rheological data of polymer melts long ago by Ferry [115]. The curves in Fig. 27b show a similar shape for curves measured at different temperatures or MWCNT content. Although the shear rates are limited in our experiments to a maximum of 1 s^{-1} it seems to be possible to predict (e.g. for FEM simulations) a larger range of shear rates. An extension of the shear rate up to 300 s^{-1} for 2 wt% MWCNT and 340 °C is already close to the conditions in the injection molding process. Our 'master curve construction' assumes that for the same (steady state) conductivity at higher temperatures (i.e. lower viscosities) or higher MWCNT contents higher shear rates are required, but that the underlying mechanisms of destruction and build-up of the filler network are the same. Similar to the 'thermo-rheological simplicity' for rheological master plots [115] one may introduce here a 'thermo-rheo-electrical simplicity'.

4.6. Oscillatory shear

In the previous sections destruction and build-up of the CNT network was discussed for quasi-steady shear experiments using a rheometer with external motor control. An alternative experimental approach is the use of oscillatory shear experiments [116–118] with sufficiently high strain amplitudes to influence the CNT network (see Fig. 23, lower graph). Although, both experiments can be explained by destruction and build-up of the filler network, quite different facets are reflected. Oscillatory shear experiments can be performed using commercial rheometers with an upgrade for electrical conductivity measurements (no external motor control is needed). As mentioned above in our rheometer a ring electrode was used to guarantee an almost defined shear rate in the volume used for conductivity measurements [35,36]. In order to get sufficiently high data acquisition rates, the data were acquired using a PXI data acquisition system (National Instruments), using the analog output of an electrometer and the torque and position signals from the ARES rheometer (Fig. 28). For calculation of the strain rate, the time derivative of the position signal was taken.

The left graph in Fig. 28 shows an experiment, in which oscillatory shear strain amplitudes of 10, 100, 200, 300 and 400% (frequency of 1 s^{-1}) were successively applied to a melt with 0.6 vol%

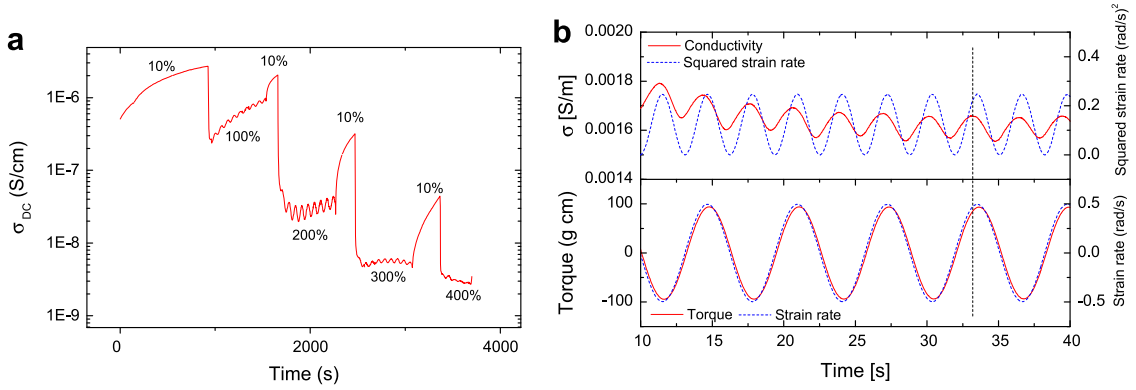

Fig. 28. (a) Electrical conductivity versus experimental time for different oscillatory shear strain for a melt with 0.6 vol% MWCNT at 230 °C (frequency of 1 Hz and different strain amplitudes, as indicated in the figure). (b) Conductivity, squared strain rate, torque and strain rate for steady-state conditions as a function of time (strain amplitude of 50%, frequency 0.16 Hz).

MWCNT at 230 °C. For recovery between the time intervals with high shear strain, a lower shear amplitude of only 10% was applied at a frequency of 1 Hz to produce a similar 'initial state'. At a first view, the conductivity in the oscillatory shear experiments shows similar features as for steady shear experiments (Section 4.5): e.g. it seems that the electrical conductivity approaches a steady-state value. In order to compare the effect of both oscillatory and steady shear, we introduced an effective shear rate $\dot{\gamma}_{eff}$ as the average of the absolute value of shear rate $\dot{\gamma}$ over one period:

$$\dot{\gamma}_{eff} = \langle|\dot{\gamma}|\rangle = \dot{\gamma}_0/\frac{\pi}{2} = \gamma_0\omega/\frac{\pi}{2}, \quad (18)$$

with $\gamma(t) = \gamma_0 \sin\omega t$, $\dot{\gamma}_0 = \gamma_0\omega$ is the shear rate amplitude, and $\langle\ldots.\rangle$ denotes the average for one period of the oscillations. By comparing oscillatory and steady shear experiments on the same composite (not shown here) with equal values of effective shear rate $\dot{\gamma}_{eff}$ (oscillatory experiment) and steady shear rate ($\dot{\gamma}_{steady}$) the conductivity decrease is considerably lower for the oscillatory experiment. This is not surprising since in the oscillatory experiment for moderate shear amplitudes the CNT network is almost reversibly deformed, whereas in the steady shear experiment the network is irreversibly deformed. This is supported by the fact that for increasing frequency the shear-induced network destruction by the oscillatory shear becomes even less pronounced, since for the same effective shear rate the shear amplitude is decreasing with higher frequencies. The frequency dependence of γ_0 is given by:

$$\gamma_0 = \frac{\dot{\gamma}_0}{\omega} = \frac{\dot{\gamma}_{eff}}{\omega}\frac{\pi}{2}, \quad (19)$$

which can be easily derived from Eq. (18) using

$$\dot{\gamma} = \dot{\gamma}_0 \cdot \cos\omega t = \gamma_0\omega \cdot \cos\omega t = \mathrm{d}(\gamma_0 \sin\omega t)/\mathrm{d}t. \quad (20)$$

A first indication for this was given by Lellinger et al. some years ago [116]. Shear induced destruction and at least partial reformation of the nanotube network by forward-backward shearing – which is very similar to oscillatory shear – has been reported in Ref. [37].

Fig. 28b shows the time-resolved dependence of the electrical conductivity during sinusoidal shear with a strain amplitude of 50% and a frequency of 1 rad/s (0.16 Hz). As it can be seen the torque is almost proportional to the strain rate (torque $\propto \tau = \eta\dot{\gamma}$), with only a minimal phase shift between the two signals. Thus, the mechanical response of the sample is nearly that of a pure viscous system. On the other hand, the electrical conductivity behaves quite different: the frequency of the conductivity change is twice the frequency of the mechanical excitation. This could be expected, if the conductivity decreases with increasing squared strain rate. Under this assumption, the conductivity should become minimal at each maximum of the squared strain rate, and would get maximal when the strain rate is zero. However our experiments show a different behavior: the conductivity reaches its minimum shortly before the strain rate gets zero, and the conductivity maximum is located close before the maximum of the squared strain rate. In terms of strain, the conductivity reaches its maximum at zero strain, and its minimum at the reversal points of the oscillation, i.e. when the strain is maximal [116]. This is different as expected for steady shear and can be explained in terms of a memory effect of the network of agglomerates. When the strain increases, the network gets partially deformed or disrupted, and the conductivity decreases. But after the reversal point of the oscillation of the strain, the agglomerates return to their old positions, re-forming the conductive network, and thus conductivity increases again. To answer the question how long this "memory effect" persists, a detailed investigation using transient shear signals was made [37].

4.7. Orientation versus agglomeration

The question, how orientation and agglomeration/de-agglomeration of nanotubes in a shear flow are related to each other is of particular interest for both, basic understanding and polymer melt processing. Despite melt deformation occurring during extrusion, the latter is of specific interest in injection molding, which is a very complex non-isothermal process with a combination of different flow fields [56]. Although elongation flow can also play an important role, we concentrate in the following only on shear flow during injection molding. On the one hand, it is established since long by theoretical considerations that rigid rods and non-spherical particles in general are oriented under simple shear flow in viscous liquids [119–122]. Furthermore, as stated already in the introduction, several authors [53–56] reported on orientation of CNTs under mechanical deformation. On the other hand, we stated in Sections 2.2. and 4.2. that the competition between agglomeration and de-agglomeration is the dominant factor for the final properties of CNTs dispersed in a polymer matrix. In injection molded samples orientation can regarded as an effect of second order when applying moderate flow/processing conditions ($\dot{\gamma} < 10^2\ s^{-1}$). This seems to be at least partially supported by compression molding and micro-injection molding experiments of Abbasi et al. [56] on MWCNTs in PC, where CNT alignment in the inner part of the samples was only indicated for the very high shear rates during micro-injection molding ($\dot{\gamma} \approx 10^5$–$10^9\ s^{-1}$) and almost no alignment was found for compression molded composites. This is consistent to our findings for compression molded plates (see Fig. 17), where only agglomeration was indicated [57]. However, detailed TEM investigations near the wall of the mold clearly indicated nanotube alignment within a surface layer of about 20 μm, as shown in the left TEM micrograph in Fig. 29 [123]. This image represents a cut taken at a depth of 2 μm from the sample surface of an injection molded plate with 2 wt% MWCNT in PC where the orientation induced during injection of the filled melt is frozen immediately due to the cold mold wall. Such frozen orientations can be also observed in melt spun fibers produced at high take-up velocities and fast polymer matrix vitrification, as e.g. reported on PC based fibers with MWCNTs produced with take-up velocities up to 800 m/s [124]. However, when looking in the injection molded sample in distances well apart from the wall, no CNT alignment is obvious, as shown in the right micrograph of Fig. 29 (cut from a depth of 23 μm). These findings show that the CNT orientation in injection

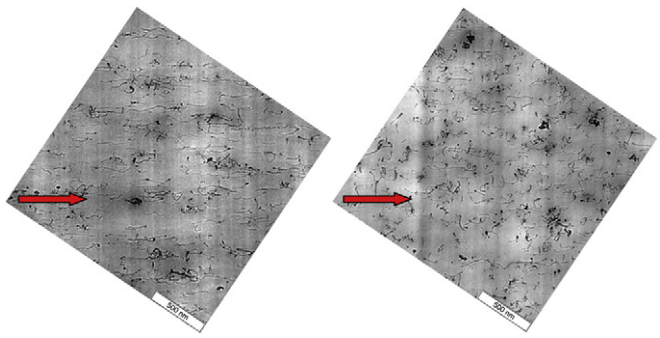

Fig. 29. TEM micrograph of ultrathin cuts (cuts perpendicular to the plate surface) of an injection molded plate with 2 wt% MWCNT in PC for different depths from the surface (center of the cut at a depth of left figure: 2 μm; right figure: 23 μm). The flow direction is indicated by arrows. Replotted from Ref. [123].

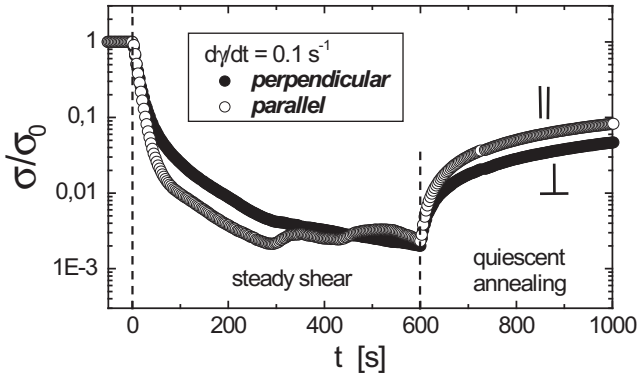

Fig. 30. Normalized conductivity parallel (solid symbols) and perpendicular (open symbols) to the shear flow for PC with 1 wt% MWCNT (Baytubes® C150P) in the melt at 230 °C after isothermal annealing ($t > 0$), during steady shear deformation ($0 \text{ s} < t < 600 \text{ s}$) and for annealing in the quiescent melt ($t > 600$ s).

molding has to be taken into consideration only at very high shear rates and high viscous or highly elastic polymer melts in a comparatively very small volume close to the sample surface and therefore is regarded as an effect of second order at moderate shear rates in the bulk.

In the more fundamental works on CNT orientation of Hobbie et al. [53,54] on low viscous and weakly elastic polymer melts of low molecular weight and semidilute dispersion (0.17 wt%) of the MWCNTs the orientation of CNTs along the direction of flow has been found at low shear stress. Furthermore, a transition to vorticity alignment above a critical shear stress, corresponding to a critical Deborah number, has been indicated by using a small angle-light scattering/microscopy instrument. In this experiment, polybutadiene of very low molecular weight and dilute suspensions were studied. However, the authors themselves argued that shear can induce agglomeration of non-Brownian nanofibers and that the MWCNT agglomerates can be "molten" above a critical shear stress. In a more recent paper by Pujari et al. [55] on MWCNTs in uncured epoxy resins of low viscosity by small-angle X-ray scattering experiments it was also hypothesized, that the shear rate dependence of CNT orientation is somehow coupled to the what we call "agglomeration/de-agglomeration" of nanotubes. However, one can assume, that the interplay of agglomeration/de-agglomeration and CNT orientation depend on many factors like matrix viscosity and elasticity, shear rate, aspect ratio and attractive/repulsive interaction of the nanofiller. We speculate, that for low or moderate shear rates/stresses and/or moderate CNT concentration (rather typical for melt processing) agglomeration/de-agglomeration is dominant, whereas for very low CNT loadings and/or higher shear rates/stresses orientation effects become more important (e.g. solution or melt spinning, injection molding near the wall of a mold).

In order to investigate the interplay of orientation and agglomeration/de-agglomeration on the electrical conductivity, we performed rheo-electrical model experiments with circular finger electrodes parallel and perpendicular to the flow direction [125,126]. For these experiments the rheo-electrical setup described above was used.

Fig. 30 shows the normalized DC conductivity (actual conductivity divided by the conductivity at $t = 0$) for PC with 1 wt% MWCNT (Baytubes® C150P) in the melt at 230 °C after annealing of the as received sample ($t > 0$), during steady shear deformation ($0 \text{ s} < t < 600$ s) and for annealing in the quiescent melt (conductivity recovery) for $t > 600$ s. The normalization was used to reduce small electrical asymmetries between the parallel and perpendicular electrode arrangements (the absolute conductivity after annealing for both directions was about 6×10^{-2} S/m). It is seen that the conductivities parallel and perpendicular to the shear direction show the same trends. The differences between both directions are not significant and in the order of the experimental error. The experimental error is indicated by the amplitude of the "oscillation" of the curve for the conductivity parallel to the flow direction.

Since during steady shear no significant difference between both directions can be detected and the destruction and recover kinetics (decay of both curves) is similar, one can conclude, that the conductivity does not show significant orientation effects. Since the conductivity is extremely dependent on the CNT arrangement, this can be taken as a further indication for the minor effect of CNT alignment for moderate shear conditions. The same trends were found for carbon black in PC, indicating that there is almost no influence of the aspect ratio on the case of agglomeration/de-agglomeration [125,126].

4.8. Destruction and build-up of the filler network during injection molding

As stated above, polymer melts containing CNTs undergo mechanical deformations during compounding, extrusion and

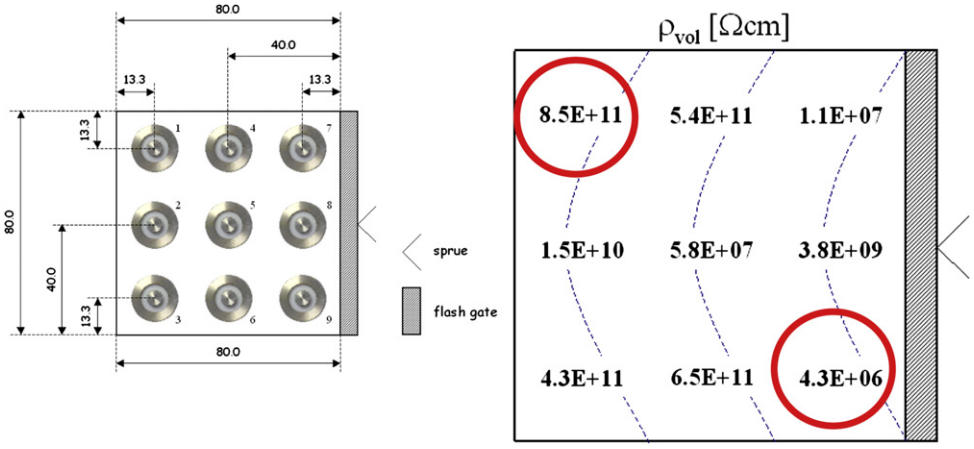

Fig. 31. Positions of volume resistance sensors on an injection molded plate ($80 \times 80 \times 2$ mm^3) (left) and the volume resistivity measured through the plate (right) for a given set of processing conditions (see Ref. [123]). The largest difference is indicated by red circles.

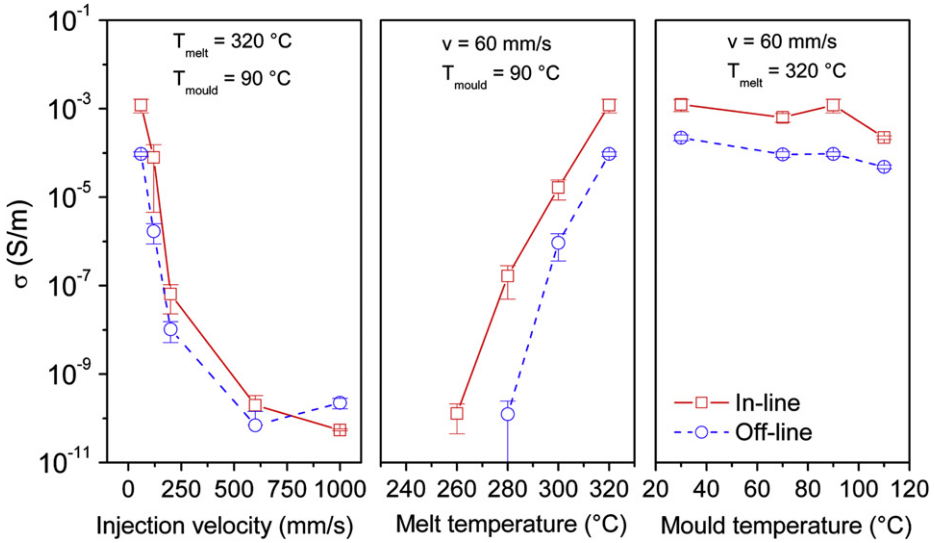

Fig. 32. Influence of injection speed v (left), melt temperature (middle) and mold temperature T_{mold} (right) on the in-line and off-line measured electrical conductivity of a polycarbonate/styrene-co-acrylnitrile blend (Bayblend®) containing 4 wt% MWCNT. Replotted from Ref. [127].

injection molding which affect the state of filler network [7,12,34,123,127]. This state of the nanotube network - which is induced by processing of the polymer melt and frozen ("frustrated") in the short period prior to vitrification or crystallization - mainly defines the physical properties of the final plastic part. Parallel to the laboratory experiments the influence of shear and elongation flow on the electrical conductivity of CNT-polymer composites has been found as well in processing related studies [12,34,57,67,123,127] during extrusion, pressing and injection molding. The destruction of the conductive filler network by mechanical deformation (nanotube de-agglomeration and/or orientation) was observed for the first time in in-line conductivity experiments during extrusion of PP [12], PC and PA 6 [34] containing different amounts of MWCNTs. As discussed already above (see Fig. 17), Pegel et al. [57] showed examples for deformation-induced agglomeration of CNTs in PC composites in the squeeze flow during compression molding. Villmow et al. [67,123] demonstrated the destructive effect of mechanical deformation on the electrical conductivity of injection molded plastic parts. In Fig. 31 [123] a conductivity variation up to 5 orders of magnitude within the same injection molded PC/MWCNT plate was found and related to different flow conditions.

Similar results were obtained by in-line and off-line conductivity measurements during and after injection molding of samples of PC/MWCNT, PA/MWCNT and an acrylonitrile-butadiene-styrene/polycarbonate blend (Bayblend™) with MWCNT for a wide variation of the processing parameters [127]. For time-resolved in-line measurements of the DC conductivity during injection molding an injection molding machine (Klöckner Ferromatik Desma FX75-2F, Germany) was equipped with a mold containing three borings on every side to accommodate conductivity and/or pressure sensors in different arrangements [127]. The corresponding off-line measurements of the conductivities at the same locations of the final parts were conducted using two opposing electrodes. The geometrical factors to calculate the specific electrical conductivities for in-line and off-line electrode configuration were calculated by FEM.

In Fig. 32 as an example the in-line conductivity data of injection molding of Bayblend® with 4 wt% MWCNT are shown together with off-line measured values for different injection velocities, melt and mold temperatures. Very similar results are found for matrices

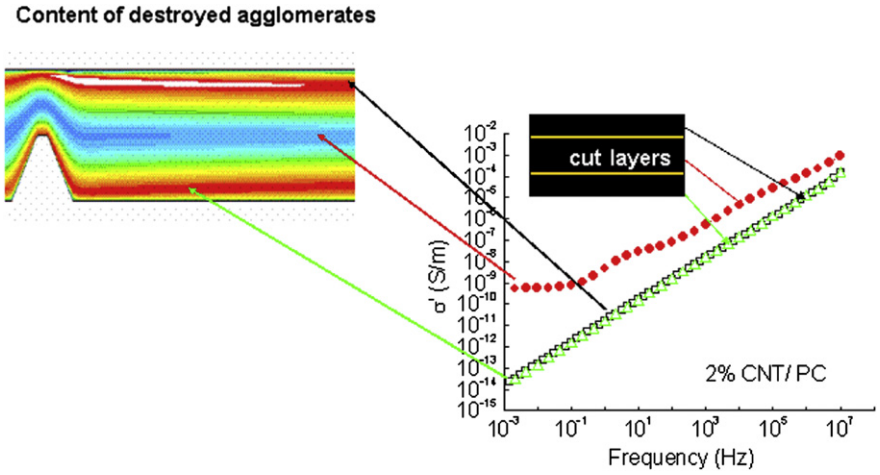

Fig. 33. Layer structure in an injection molded plate: Off-line measured frequency dependent conductivity for the middle and the outer layers ('cuts) of a PC containing 2 wt% MWCNT (right) and the simulated amount of destroyed agglomerates (increasing from blue to red). Replotted from Refs. [114,128].

of amorphous homopolymer (PC) and a semi-crystalline polymer (PA) [127]. The strong dependence of the conductivity on injection velocity, melt temperature and the related viscosity can be explained by the competition between deformation-induced formation and destruction of the conductive CNT network. The electrical conductivity was recorded during a typical injection cycle (not shown). For further details see Ref. [127]. For the in-line conductivity data in Fig. 32 the values recorded 9 s after start of injection were taken, which reflect an almost vitrified state.

The good correlation between in-line and off-line data supports the assumption that the in-line values after 9 s represent already a vitrified (glassy frozen) sample. The same was found for semi-crystalline PA [127] were the measured values after about 10 s represent a semi-crystalline state. The tremendous decrease of the conductivity with increasing injection speed and decreasing temperature can be explained by the dominance of destruction of the conductive filler network due to increasing shear stress either because of an increasing shear rate (with injection velocity) or because of increasing viscosity (with temperature decrease). The relatively high conductivity values at low injection velocities and high melt temperatures cannot be explained by the destructive effect of shear deformation alone.

Therefore, we assume that the measured conductivity values in the solidified state represent the "frustrated" conductivity values resulting from the competition of deformation-induced build-up and destruction along the injection track. No significant effect of the mold temperature has been found. Since the mold temperature determines mainly the averaged cooling rate for the "frustration" of the filler network by vitrification or crystallization, this finding support our assumption that the conductivity values are mainly determined by the flow conditions and that the time for conductivity recovery is to short for typical injection cycles.

In Fig. 33 the layer structure in an injection molded plate due to competition of destruction and build-up of agglomerates in the injection molding process is illustrated [128]. The lower right part shows off-line measured frequency dependent conductivities for three parallel 'cuts' from an injection molded plate of a PC containing 2 wt% MWCNT. The conductivity of the middle layer ('cut') is considerable higher than that of the outer layers. This is supported by an FEM simulation (upper right graph) of the destroyed agglomerates [114] using similar models (combination of agglomeration kinetics and 'percolation equation') as explained above.

5. Concluding remarks

It was generally assumed that nanofillers have to be well dispersed in the polymer matrix to achieve the desired properties or property combinations. Therefore, much effort is usually spent during polymer melt processing or in sample preparation (melt mixing, compounding, dispersion in a thermosetting matrix etc.) to disintegrate the *initial agglomerates* in which most of the nanofiller materials are produced. It is further assumed that the high specific surface of the nanofillers creates in the polymer matrix a large amount of an interphase with different properties, which may involve the total volume of the matrix polymer. This interphase contributes to improvement of mechanical properties like impact stress or in some cases of stiffness and elongation at break. However, for the well dispersed (and homogeneously distributed) nanotubes the measured electrical conductivity of the composites is in the order of the conductivity of the neat polymer. The same holds true for other conductive fillers like carbon black.

By thermal annealing in the quiescent melt (absence of shear) a *secondary agglomeration* (or cluster formation) of nanotubes and formation of a conductive network of interconnected agglomerates [31–34] could be found, which leads to an increase of the conductivity of the composite melt by several orders of magnitude. Furthermore, shear flow can both generate and destroy secondary agglomerates. On the one hand, agglomeration or cluster formation is further accelerated by shear flow. On the other hand, since secondary agglomerates are more loosely packed than initial agglomerates, they can be easily destroyed by shear treatment. Therefore, the competition between build-up and destruction of secondary agglomerates (or physical clusters) is considered as a key mechanism to understand the dependence of the final properties (here: electrical conductivity) on the thermal and rheological prehistory (preparation or processing conditions). The increase of the conductivity with annealing time is discussed in terms of a time-dependent insulator-conductor transition due to nanotube agglomeration [32].

The main results can be summarized as follows:

(1) To achieve a polymer/carbon nanotube composite with high electrical conductivity the *initial agglomerates* have first to be dispersed in the polymer matrix to get well separated nanotubes, which can then rearrange to *secondary agglomerates* forming the conductive filler network.
(2) The process of nanotube dispersion within a polymer matrix by melt mixing was illustrated and discussed in terms of different steps and mechanisms: agglomerate *wetting* and *infiltration* by the matrix polymer and *rupture* and *erosion* of the initial agglomerates.
(3) Secondary agglomeration of attractive filler particles is assumed to be a thermally activated process and can be accelerated by shear (and elongational) flow.
(4) The time dependence of electrical conductivity, storage (G') and loss modulus (G'') in the quiescent melt and under quasi-steady shear or oscillatory shear conditions are explained by build-up and destruction of a network formed by CNT agglomerates. The competition between formation and destruction of agglomerates under shear can be described by kinetic models.
(5) By combining agglomeration kinetics and an equation for the insulator-conductor transition the electrical conductivity in composites containing conductive fillers can be described. The model was incorporated into FEM code.
(6) The mechanisms of charge carrier transport in a nanotube network and the effect of mechanical reinforcement are found to be different. The best isotropic mechanical reinforcement is expected for randomly distributed nanotubes forming a combined viscoelastic nanotube-polymer network, whereas for good electrical conductivity secondary agglomeration and small CNT–CNT distances are necessary.

The results reported here for carbon nanotubes in polymers or thermosets seem to have general importance for filler networks in viscoelastic or viscous matrices. Apart from its scientific interest the results can help to optimize industrial production of polymer/nanotube composites.

Acknowledgments

Part of the work was funded by the German Federal Ministry of Education and Research (BMBF) in the WING Program "Virtual Material Development" (CarboNet, funding No. 03X0504E) and in the Framework Concept "Research for Tomorrows Production" (COMPOMEL, funding No. 02PU2394). Furthermore we thank the Bundesministerium für Wirtschaft (German Federal Ministry for Economic Affairs) via the Arbeitsgemeinschaft Industrieller Forschungsgesellschaften (AiF) for financial support of the AiF projects No. 122Z and 14454N. We would like to acknowledge the

contributions of W. Böhm, Dr. M. Engel and A. Bormuth (DKI) to dielectric and rheological results and of R. Boldt and Dr. B. Krause (IPF) to measurements of the nanotube length distributions. We thank Dr. M. Bierdel (Bayer Technology Services), Dr. H. Meyer (Bayer MaterialScience AG) and Dr. S. Hermasch (Evonik Industries AG, Marl, Germany) for providing part of the samples. Furthermore, we would like to thank Hyperion Catalysis International, Inc. (Cambridge, USA) for providing MWCNT masterbatches. We acknowledge the contributions of Dr. M. Engel (DKI, TU Darmstadt), Dr. D. Xu, A. Ohneiser, H. Dörr, F. Pfleger and G. Vulpius (DKI) to the in-line experiments. We also thank Prof. G. Heinrich and Dr. M. Grenzer (IPF) for helpful discussions. In addition, we thank an unknown referee for very helpful comments and discussion.

References

[1] Radushkevich LV, Lukyanovich VM. Zhurnal Fizicheskoi Khimii 1952;26:88–95.
[2] Iijima S. Nature 1991;354(6348):56–8.
[3] Tennent HG. Carbon fibrils, method for producing same and compositions containing same. Patent 4 663 230. Andover, MA: US Hyperion Catalysis International, Inc.; 1984.
[4] Ajayan PM, Zhou OZ. Applications of carbon nanotubes. In: Dresselhaus MS, Dresselhaus G, Avouris P, editors. Topics in applied physics, vol. 80. Berlin Heidelberg New York: Springer Verlag; 2001. p. 391–425.
[5] Coleman JN, Khan U, Gun'ko YK. Advanced Materials 2006;18(6):689–706.
[6] Szleifer I, Yerushalmi-Rozen R. Polymer 2005;46(19):7803–18.
[7] Alig I, Pötschke P, Pegel S, Dudkin S, Lellinger D. Rubber Fiber Plastics 2008;3(2):92–5.
[8] Pötschke P, Dudkin SM, Alig I. Polymer 2003;44(17):5023–30.
[9] Schueler R, Petermann J, Schulte K, Wentzel HP. Macromolecular Symposia 1996;104:261–8.
[10] Schueler R, Petermann J, Schulte K, Wentzel HP. Journal of Applied Polymer Science 1997;63(13):1741–6.
[11] Coleman JN, Curran S, Dalton AB, Davey AP, McCarthy B, Blau W, et al. Physical Review B 1998;58(12):R7492–5.
[12] Alig I, Lellinger D, Dudkin SM, Pötschke P. Polymer 2007;48(4):1020–9.
[13] Sandler JKW, Kirk JE, Kinloch IA, Shaffer MSP, Windle AH. Polymer 2003;44(19):5893–9.
[14] Bauhofer W, Kovacs JZ. Composites Science and Technology 2009;69(10):1486–98.
[15] An KH, Jeong SY, Hwang HR, Lee YH. Advanced Materials 2004;16(12):1005–9.
[16] Villmow T, Pegel S, Pötschke P, Heinrich G. Polymer 2011;52(10):2276–85.
[17] Russell JM, Oh SJ, LaRue I, Zhou O, Samulski ET. Thin Solid Films 2006;509(1–2):53–7.
[18] Carroll DL, Czerw R, Webster S. Synthetic Metals 2005;155:694–7.
[19] Li C, Thostenson ET, Chou TW. Composites Science and Technology 2008;68(6):1227–49.
[20] Kang IP, Heung YY, Kim JH, Lee JW, Gollapudi R, Subramaniam S, et al. Composites Part B-Engineering 2006;37(6):382–94.
[21] Pötschke P, Abdel-Goad M, Alig I, Dudkin S, Lellinger D. Polymer 2004;45(26):8863–70.
[22] Klüppel M. Advances in Polymer Science 2003;164:1–86.
[23] Meincke O, Kaempfer D, Weickmann H, Friedrich C, Vathauer M, Warth H. Polymer 2004;45(3):739–48.
[24] Li CY, Thostenson ET, Chou TW. Applied Physics Letters 2007;91(22).
[25] Doi M, Edwards SF. The theory of polymer dynamics. Oxford: Clarendon Press; 1986.
[26] Kyrylyuk AV, van der Schoot P. Proceedings of the National Academy of Sciences of the United States of America 2008;105(24):8221–6.
[27] Balberg I, Binenbaum N, Wagner N. Physical Review Letters 1984;52(17):1465–8.
[28] Balberg I, Anderson CH, Alexander S, Wagner N. Physical Review B 1984;30(7):3933–43.
[29] Balberg I. Philosophical Magazine B-Physics of Condensed Matter Statistical Mechanics Electronic Optical and Magnetic Properties 1987;56(6):991–1003.
[30] Bryning MB, Islam MF, Kikkawa JM, Yodh AG. Advanced Materials 2005;17(9):1186–91.
[31] Alig I, Skipa T, Engel M, Lellinger D, Pegel S, Pötschke P. Physica Status Solidi B-Basic Solid State Physics 2007;244(11):4223–6.
[32] Alig I, Skipa T, Lellinger D, Bierdel M, Meyer H. Physica Status Solidi B-Basic Solid State Physics 2008;245(10):2264–7.
[33] Alig I, Skipa T, Lellinger D, Pötschke P. Polymer 2008;49(16):3524–32.
[34] Alig I, Lellinger D, Engel M, Skipa T, Pötschke P. Polymer 2008;49(7):1902–9.
[35] Skipa T, Lellinger D, Saphiannikova M, Alig I. Physica Status Solidi B-Basic Solid State Physics 2009;246(11–12):2453–6.
[36] Skipa T, Lellinger D, Böhm W, Saphiannikova M, Alig I. Polymer 2010;51(1):201–10.
[37] Lellinger D, Skipa T, Böhm W, Alig I. Physica Status Solidi B-Basic Solid State Physics 2009;246(11–12):2667–70.
[38] Heinrich G, Costa FR, Abdel-Goad M, Wagenknecht U, Lauke B, Härtel V, et al. Kautschuk Gummi Kunststoffe 2005;58(4):163–7.
[39] Hobbie EK, Fry DJ. Journal of Chemical Physics 2007;126(12).
[40] Lin-Gibson S, Pathak JA, Grulke EA, Wang H, Hobbie EK. Physical Review Letters 2004;92(4).
[41] Hobbie EK, Fry DJ. Physical Review Letters 2006;97(3).
[42] Kovacs JZ, Velagala BS, Schulte K, Bauhofer W. Composites Science and Technology 2007;67(5):922–8.
[43] Ma AWK, Mackley MR, Rahatekar SS. Rheologica Acta 2007;46(7):979–87.
[44] Sandler JKW, Windle AH, Martin CA, Schwarz ML, Bauhofer W, Schulte K, et al. Continuous Nanophase and Nanostructured Materials 2004;788:221–6.
[45] Martin CA, Sandler JKW, Shaffer MSP, Schwarz MK, Bauhofer W, Schulte K, et al. Composites Science and Technology 2004;64(15):2309–16.
[46] Guery J, Bertrand E, Rouzeau C, Levitz P, Weitz DA, Bibette J. Physical Review Letters 2006;96(19).
[47] Vermant J, Solomon MJ. Journal of Physics-Condensed Matter 2005;17(4):R187–216.
[48] Switzer LH, Klingenberg DJ. International Journal of Multiphase Flow 2004;30(1):67–87.
[49] Hobbie EK, Jeon HS, Wang H, Kim H, Stout DJ, Han CC. Journal of Chemical Physics 2002;117(13):6350–9.
[50] Han CC, Yao YH, Zhang RY, Hobbie EK. Polymer 2006;47(10):3271–86.
[51] Li C, Thostenson ET, Chou TW. Composites Science and Technology 2008;68(6):1445–52.
[52] Krause B, Boldt R, Pötschke P. Carbon 2011;49(4):1243–7.
[53] Hobbie EK, Wang H, Kim H, Han CC, Grulke EA, Obrzut J. Review of Scientific Instruments 2003;74(3):1244–50.
[54] Hobbie EK, Wang H, Kim H, Lin-Gibson S, Grulke EA. Physics of Fluids 2003;15(5):1196–202.
[55] Pujari S, Rahatekar SS, Gilman JW, Koziol KK, Windle AH, Burghardt WR. Journal of Chemical Physics 2009;130(21).
[56] Abbasi S, Carreau PJ, Derdouri A. Polymer 2010;51(4):922–35.
[57] Pegel S, Pötschke P, Petzold G, Alig I, Dudkin SM, Lellinger D. Polymer 2008;49(4):974–84.
[58] Castillo FY, Krause B, Headrick R, Grad BP, Prada-Silvy R, and Pötsche P. Polymer 2011:(submitted).
[59] Data sheet nanocyl NC 7000. Sambreville, Belgium: Nanocyl; 2010.
[60] Datasheet baytubes C150P. Bayer MaterialScience AG; 2009.
[61] Krause B, Mende M, Pötschke P, Petzold G. Carbon 2010;48(10):2746–54.
[62] Barber AH, Cohen SR, Wagner HD. Physical Review Letters 2004;92:186103–4.
[63] Rumpf HCH. Chemie Ingenieur Technik 1970;42(8):538–40.
[64] Ottino JM, DeRoussel P, Hansen S, Khakhar DV. Mixing and dispersion of viscous liquids and powdered solids. In: James W, editor. Advances in chemical engineering, vol. 25. Academic Press; 1999. p. 105–204.
[65] Krause B, Pötschke P, Häußler L. Composites Science and Technology 2009;69(10):1505–15.
[66] Kasaliwal GR, Pegel S, Göldel A, Pötschke P, Heinrich G. Polymer 2010;51(12):2708–20.
[67] Villmow T, Pötschke P, Pegel S, Häußler L, Kretzschmar B. Polymer 2008;49(16):3500–9.
[68] Kasaliwal GR, Pötschke P, Göldel A, Heinrich G. Polymer 2011;52(4):1027–36.
[69] Li J, Ma PC, Chow WS, To CK, Tang BZ, Kim JK. Advanced Functional Materials 2007;17(16):3207–15.
[70] Kashiwagi T, Fagan J, Douglas JF, Yamamoto K, Heckert AN, Leigh SD, et al. Polymer 2007;48(16):4855–66.
[71] Le HH, Kasaliwal G, Ilisch S, Radusch HJ. Kgk-Kautschuk Gummi Kunststoffe 2009;62(6):326–33.
[72] Kasaliwal G, Göldel A, Pötschke P. Journal of Applied Polymer Science 2009;112(6):3494–509.
[73] Pegel S, Villmow T, Pötsche P. Quantification of dispersion and distribution of carbon nanotubes in polymer composites using microscopy techniques. In: McNally T, Pötschke P, editors. Polymer-carbon nanotube composites: preparation, properties and applications. Oxford: WP, Woodhead Publ; 2011. p. 265–94.
[74] Stoyan D, Kendall WS, Mecke J. Stochastic geometry and its applications. Chichester [U.A.]: Wiley; 1987.
[75] Socher R, Krause B, Boldt R, Hermasch S, Wursche R, Pötschke P. Composites Science and Technology 2011;71(3):306–14.
[76] Kasaliwal G, Villmow T, Pegel S, Pötsche P. Influence of material and processing parameters on carbon nanotube dispersion in polymer melts. In: McNally T, Pötschke P, editors. Polymer-carbon nanotube composites: preparation, properties and applications. Oxford [U.A.]: WP, Woodhead Publ.; 2011. p. 92–132.
[77] Pegel S. Komposite aus Polycarbonat und Kohlenstoff-Nanoröhren: Morphologie und elektrische Leitfähigkeit bei thermoplastischer Verarbeitung. PhD thesis. Germany: Technical University of Dresden; 2011.
[78] Pötschke P, Bhattacharyya AR, Janke A, Pegel S, Leonhardt A, Taschner C, et al. Fullerenes Nanotubes and Carbon Nanostructures 2005;13:211–24.
[79] Mičušik M, Omastová M, Krupa I, Prokeš J, Pissis P, Logakis E, et al. Journal of Applied Polymer Science 2009;113(4):2536–51.

[80] Krause B, Petzold G, Pegel S, Pötschke P. Carbon 2009;47(3):602–12.
[81] Pegel S, Villmow T, Kasaliwal G, Pötsche P. Polymer-carbon nanotube composites: melt processing, properties and applications. In: Bhattacharyya D, Fakirov S, editors. Synthetic all-polymer composites. Munich: Hanser Publishers; 2011.
[82] Villmow T, Kretzschmar B, Pötschke P. Composites Science and Technology 2010;70(14):2045–55.
[83] Müller MT, Krause B, Kretzschmar B, Pötschke P. Composites Science and Technology; 2011.
[84] McClory C, Pötschke P, McNally T. Macromolecular Materials and Engineering 2011;296(1):59–69.
[85] Krause B, Villmow T, Boldt R, Mende M, Petzold G, Pötschke P. Composites Science and Technology 2011;71(8):1145–53.
[86] Meier JG, Klüppel M. Macromolecular Materials and Engineering 2008; 293(1):12–38.
[87] Ruschau GR, Yoshikawa S, Newnham RE. Journal of Applied Physics 1992; 72(3):953–9.
[88] Gojny FH, Wichmann MHG, Fiedler B, Kinloch IA, Bauhofer W, Windle AH, et al. Polymer 2006;47(6):2036–45.
[89] Gojny FH, Wichmann MHG, Fiedler B, Schulte K. Composites Science and Technology 2005;65(15–16):2300–13.
[90] Kharchenko SB, Douglas JF, Obrzut J, Grulke EA, Migler KB. Nature Materials 2004;3(8):564–8.
[91] Obrzut J, Douglas JF, Kharchenko SB, Migler KB. Physical Review B 2007; 76(19).
[92] Bauhofer W, Schulz SC, Eken AE, Skipa T, Lellinger D, Alig I, et al. Polymer 2010;51(22):5024–7.
[93] Kirkpatrick S. Reviews of Modern Physics 1973;45(4):574–88.
[94] De Gennes PG. Journal de Physique Letters 1976;37 (Paris).
[95] Efros AL, Shklovskii BI. Physica Status Solidi B-Basic Research 1976;76(2): 475–85.
[96] Straley JP. Journal of Physics C-Solid State Physics 1976;9(5):783–95.
[97] Bergman DJ, Imry Y. Physical Review Letters 1977;39(19):1222–5.
[98] Webman I, Jortner J, Cohen MH. Physical Review B 1977;16(6): 2593–6.
[99] Clerc JP, Giraud G, Laugier JM, Luck JM. Advances in Physics 1990;39(3): 191–308.
[100] Bunde A, Havlin S. Fractals and disordered systems. Berlin-Heidelberg-New York: Springer; 1996.
[101] Stauffer D, Aharony A. Introduction to percolation theory. London: Taylor & Francis Ltd.; 1994.
[102] Sahimi M. Applications of percolation theory. London: Taylor & Francis Ltd.; 1994.
[103] McLachlan DS, Blaszkiewicz M, Newnham RE. Journal of the American Ceramic Society 1990;73(8):2187–203.
[104] Andrews R, Jacques D, Qian D, Dickey EC. Carbon 2001;39(11):1681–7.
[105] Almond DP, Bowen CR. Physical Review Letters 2004;92(15).
[106] Fournier J, Boiteux G, Seytre G, Marichy G. Synthetic Metals 1997;84(1–3): 839–40.
[107] Curran SA, Zhang DH, Wondmagegn WT, Ellis AV, Cech J, Roth S, et al. Journal of Materials Research 2006;21(4):1071–7.
[108] McCullen SD, Stevens DR, Roberts WA, Ojha SS, Clarke LI, Gorga RE. Macromolecules 2007;40(4):997–1003.
[109] Deng H, Skipa T, Zhang R, Lellinger D, Bilotti E, Alig I, Peijs T. Polymer 2009; 50(15):3747–54.
[110] Pötschke P, Fornes TD, Paul DR. Polymer 2002;43(11):3247–55.
[111] Du FM, Scogna RC, Zhou W, Brand S, Fischer JE, Winey KI. Macromolecules 2004;37(24):9048–55.
[112] Martins JN, Bassani TS, Barra GMO, Oliveira RVB. Polymer International 2011; 60(3):430–5.
[113] Tanner RI. Engineering rheology. 2nd ed. Oxford [u.a.]: Oxford Univ. Pr; 2000.
[114] Lellinger D, Skipa T, Saphiannikova M, Conzen C, Meyer H, Alig I. GAK Gummi Fasern Kunststoffe 2011;64(9):550–3.
[115] Ferry JD. Viscoelastic properties of polymers. 3rd ed. New York [u.a.]: Wiley; 1980.
[116] Lellinger D, Skipa T, Böhm W, and Alig I. Abstract book "XXIII International Winterschool on electronic properties of novel materials" in Kirchberg/Tirol, 7–14. March 2009; Poster II-28:100-101.
[117] Handge UA, Zeiler R, Dijkstra DJ, Meyer H, Altstädt V. Polymer 2011;52(2): 430–42.
[118] Palza H, Kappes M, Hennrich F, Wilhelm M. Composites Science and Technology 2011;71(10):1361–6.
[119] Jeffery GB. Proceedings of the Royal Society of London. Series A, Containing Papers of a Mathematical and Physical Character 1922;102(715): 161–79.
[120] Trevelyan BJ, Mason SG. Journal of Colloid Science 1951;6(4):354–67.
[121] Forgacs OL, Mason SG. Journal of Colloid Science 1959;14(5):457–72.
[122] Hinch EJ, Leal LG. Journal of Fluid Mechanics 1972;52:683. Apr25.
[123] Villmow T, Pegel S, Pötschke P, Wagenknecht U. Composites Science and Technology 2008;68(3–4):777–89.
[124] Pötschke P, Brünig H, Janke A, Fischer D, Jehnichen D. Polymer 2005;46(23): 10355–63.
[125] Bormuth A. Anisotropie der elektrischen Leitfähigkeit in Polymerkompositen. Fachbereich Physik, Diploma thesis. Darmstadt: Deutsches Kunststoff-Institut/Technische Universität Darmstadt; 2008.
[126] Bormuth A, Lellinger D, Skipa T, and Alig I. 2011:(in preparation).
[127] Lellinger D, Xu DH, Ohneiser A, Skipa T, Alig I. Physica Status Solidi B-Basic Solid State Physics 2008;245(10):2268–71.
[128] Xu D, Lellinger D, and Alig I. Unpublished results. 2009.

Dr. Ingo Alig is the head of the department of physical characterization at the Deutsche Kunststoff-Institut (German Institute for Polymers, DKI) and lecturer at the University of Technology of Darmstadt. He and his associates have published more than 120 papers in various areas of polymer physics and chemical physics. Another area of interest is in-line process control during polymer processing. He received his Diploma, a Ph.D., and a D.Sc. in experimental physics from the Technical University in Merseburg. He was a visiting scientist at the Research Center of Crete, the Max Planck Institute for Polymer Science in Mainz, and the McMasters University in Hamilton. From 1991 to1993, he spent two years at the department of chemical physics at the University of Cologne.

Dr. Petra Pötschke heads the research group "Composites and blends containing carbon nanofillers" at Leibniz-Institut für Polymerforschung Dresden e. V., (Leibniz Institute of Polymer Research Dresden, IPF), Germany. She studied mechanical process engineering at Dresden University of Technology in Germany and completed her PhD in 1988. Since 1988, she has been working as a scientist in the Department of Polymer Reactions and Blends at IPF Dresden, Germany. Her main research interest is in the field of multicomponent polymer based materials. In 2000/2001 she worked with Prof. Donald R. Paul at the University of Texas at Austin (Texas, USA) at the Chemical Engineering Department on multiphase blend systems, which was supported by the grant scheme of the Max-Kade Foundation, New York. Since then she has focused on carbon nanotube-filled composites and blends and their applications.

Dr. Dirk Lellinger has been a senior scientist at the Deutsche Kunststoff-Institut (German Institute for Polymers) in Darmstadt, Germany, since 1995. His primary interests are ultrasonic spectroscopy, dynamic-mechanical spectroscopy, and the development of measurement systems for laboratory automation and in-line process control. He received his Diploma and a Ph.D. from the Technical University in Merseburg. From 1993 to 1995, he spent two years at the department of physics at the University of Halle.

Dr. Tetyana Skipa graduated from Faculty of Physics of Taras Shevchenko National University of Kiew (Ukraine) with the master degree in physics in 1993. In 2001 she worked as a research assistant in the Bio-reliability group of IPCP RAS (Chernogolovka) studying the electronic properties of endohedral fullerenes in organic solutions and polymer films. Since 2002, as a PhD student she was investigating optical-electronic properties of nano-structured materials in the Institute for Solid-State Physics at the Karlsruhe Institute of Technology and received her Ph.D. degree from the Faculty of Physics of the University of Karlsruhe in 2006. Since 2006 she was post-doc researcher at the Deutsche Kunststoff-Institut (German Institute for Polymers) in Darmstadt. Her main research interests are focused on rheological and conductive properties of polymer nanocomposites.

Sven Pegel received a Diploma in mechanical engineering with the subject materials science from the Technical University Hamburg-Harburg (2003). After working as research associate in the Department of Advanced Ceramics (TUHH) he joined the group of Dr. Pötschke at the Leibniz-Institut für Polymerforschung Dresden e. V. (2004) where his research activities have been focused on the preparation, processing, and characterization of carbon nanotube polymer composites. Recently he received a Ph.D. in engineering science from Technical University Dresden (2011).

Gaurav R. Kasaliwal got a bachelor degree in chemical engineering from Shivaji University, India. He got M.Sc. in Applied Polymer Science from Martin Luther University, Halle (Saale), Germany in the year 2007. Subsequently, he joined the group of Dr. Pötschke at the Leibniz-Institut für Polymerforschung Dresden e. V. and completed his PhD research work in her group. Furthermore, he did one year post doctoral studies in the group of Prof. Gert Heinrich at IPF. He is having experience with developing multi-walled carbon nanotubes and Graphene nano platelets filled thermoplastic and elastomer composites. Recently he received a Ph.D. in engineering science from Technical University Dresden (2011). He is currently working with BASF SE, Ludwigshafen in R & D polymer research.

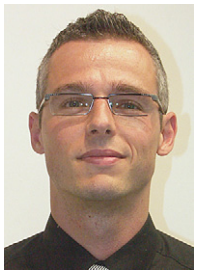

Tobias Villmow received the academic degree graduate engineer (Fachhochschule Lausitz, Senftenberg, Germany) in Mechanical Engineering in 2006. Since 2007 he has been working as scientific coworker and PhD student in the group of Dr. Pötschke at the Leibniz-Institut für Polymerforschung Dresden e. V. His fields of work are polymeric nanocomposites based on carbon nanotubes, whereas the research is focused on the investigation of processing-property relationships of melt mixed composites and their sensory behavior toward organic solvents.